

Accepted version manuscript: in Theoret. Comp. Fluid. Dyn:

DOI 10.1007/s00162-004-0155-z

## Towards a new partially integrated transport model for coarse grid and unsteady turbulent flow simulations

Roland Schiestel, Anne Dejoan\*

Institut de Recherche sur les Phénomènes Hors Equilibre, I.R.P.H.E., U.M.R. 6594 CNRS/Universités d'Aix-Marseille I & II, 49 rue Frédéric Joliot Curie, B.P. 146, Technopôle de Château-Gombert, 13384 Marseille Cedex 13, France

**Abstract.** A new two-equation model is proposed for large eddy simulations (LESs) using coarse grids. The modeled transport equations are obtained from a direct transposition of well-known statistical models by using multiscale spectrum splitting given by the filtering operation applied to the Navier–Stokes equations. The model formulation is compatible with the two extreme limits that are on one hand a direct numerical simulation and on the other hand a full statistical modeling. The characteristic length scale of subgrid turbulence is no longer given by the spatial discretization step size, but by the use of a dissipation equation. The proposed method is applied to a transposition of the well-known  $k$ - $\varepsilon$  statistical model, but the same method can be developed for more advanced closures. This approach is intended to contribute to non-zonal hybrid models that bridge Reynolds-averaged Navier–Stokes (RANS) and LES, by using a continuous change rather than matching zones. The main novelty in the model is the derivation of a new  $\varepsilon$  equation for LES that is formally consistent with RANS when the filter width is very large. This approach is dedicated to applications to non-equilibrium turbulence and coarse grid simulations. An illustration is made of large eddy simulations of turbulence submitted to periodic forcing. The model is also an alternative approach to hybrid models.

**Key words:** large eddy simulation, turbulence, subgrid scale transport model, unsteady flow, spectral non-equilibrium

**PACS:** 47.27.Eq

### 1 Introduction

The methods used in the computation of turbulent flows can be classified with respect to the range of eddies which is modeled in the turbulence spectrum. Direct numerical simulations (DNSs) require a fine grid resolution for resolving all scales of turbulence including the dissipative scales. To do so, a sufficiently precise numerical scheme is required in order to correctly capture the time evolution. When one-point models are used, the whole turbulence spectrum is modeled and the turbulence field is described through mean

---

*Correspondence to:* R. Schiestel (e-mail: Roland.Schiestel@irphe.univ-mrs.fr)

\* *Present address:* Aeronautics Department, Imperial College, London, Prince Consort, South Kensington, London SW7 2AZ, UK

values and correlations. This is a full statistical treatment of turbulence referring to transport models or algebraic models as well. The large eddy simulation (LES) approach consists of a hybrid method based on statistical modeling of the fine scales within the turbulence spectrum, whereas the large scales are computed. The fraction of the resolved scales compared to the modeled part is determined and controlled by the filtering operation applied to the Navier–Stokes equations. The usual justification of the latter method is that the fine scales are more or less universal and thus easier to model than the large scales that are dependent on the particular turbulent flow considered. A huge reduction of storage and computing time is then possible. The universality of the fine-grained turbulence remains a good approximation if the cut-off induced by the filtering operation is located within the inertial range of the spectrum. Many subgrid scale models have been proposed in the scientific literature since the first proposal by Smagorinsky, which is based on an implicit equilibrium hypothesis. Since then, more advanced models such as the dynamic model proposed by Germano et al. [16] and the structure model of Méttais and Lesieur [30], have been devised to reach greater generality in subgrid scale modeling. Another approach, first investigated by Deardorff early in 1973 (Deardorff [9]), relies on the use of transport equations for the subgrid scale Reynolds stress tensor. Several authors like Schumann [44] and Horiuti and Yoshizawa [21] have used transport equations for the turbulent kinetic energy for developing one-equation subgrid scale transport models. In these models, the characteristic turbulent length scale is in all cases, based on the cell size of the computational mesh.

However, when the mesh is coarse, the filter cutoff may be located at a wavenumber below the inertial range, and the subgrid scale turbulence may embody a part of the energy containing eddies involved in the production process. This is rather a very large eddy simulation (VLES). In this case, the hypothesis of an inertial range energy transfer based on an equilibrium hypothesis becomes questionable and there is the need to develop more advanced models. Transport equation models for subgrid scale turbulence show great promise in this prospect. The further developments of these kinds of models have been made by Krajnovic and Davidson [25] and also by Dejoan and Schiestel [13]. Considerable effort is also currently being placed on bridging Reynolds-averaged Navier–Stokes (RANS) and LES by the so-called hybrid technique (Batten et al. [3]; Davidson et al. [8]). These techniques are expected to be useful in complex flow in which a zonal approach combining RANS and LES would be relevant and is a topic of active research. An analogous point of view was developed by Hamba [17], who combined LES and RANS in channel flow calculation, the near-wall region being solved by LES whereas the standard  $k$ - $\varepsilon$  model is solved away from the wall in a one-dimensional grid. One of the problems in hybrid techniques is the difficulty to match the two regions that are described using different models. In recent work, Hamba [18] introduced a new scheme with additional filtering and succeeded to reduce the mismatch.

In the present paper, we propose the construction of a hybrid subgrid scale model, which progressively approaches a RANS model when the mesh becomes coarser. This model can be interpreted as a continuous version of a hybrid zonal approach. This idea can be related to the detached eddy simulation model DES introduced by Spalart [48]. In principle, a DES model can be derived from a RANS model by switching the statistical length scale (Travin et al. [52]) to the grid size in the wall-resolved regions of the flow. Indeed, the DES approach was originally conceived for aerodynamic flows, with juxtaposition of a thin boundary layer and a large separated region. This model is directed to operate in RANS mode by creating a RANS grid with large spacings. More recently, Nikitin et al. [33], applied the DES model as a subgrid scale model in LES of channel flow and obtained fairly accurate results.

We explore here the possibility of developing a  $k$ - $\varepsilon$ -type subgrid scale model that could be applied both to RANS and LES in a hybrid non-zonal approach (see Hanjalic et al. [19]). The major ingredient of the model is a new equation for dissipation rate of turbulence energy from which the characteristic length scale of subgrid turbulence can be determined. This new approach is expected to be relevant to cases in which the filter size is no longer a representative estimate of the unresolved (subfilter) turbulence length scale. These models will also be better suited for turbulent flows with a non-equilibrium spectral distribution produced by unsteadiness in the mean or by strong spatial perturbations because they allow to take into account some aspects of turbulence history for both velocity scales and length scales of turbulence.

One relevant feature of the present method is a consistent transposition of statistical transport modeling to subgrid scale closures. This is achieved by applying the split-spectrum concept, based on the multiscale modeling approach developed by Schiestel [41, 42] to the portioned turbulence spectrum that occurs in large

eddy simulations. The derivation of a new  $\varepsilon$  equation for LES, which is formally consistent with the RANS approach, is the main original aspect of the proposed model. The method can, in principle, be extended to most of the well-known one-point closures, leading to the derivation of their subgrid scale counterpart.

So, the present model is conceived as a LES model that is allowed to behave like a RANS model when the filter is very wide.

The scope of applications of the model is concerned with the LES and the VLES performed on coarse meshes or involving turbulent flows that are out of equilibrium. In the present paper, three turbulent flows are considered to test the new method. One is the decay of homogeneous turbulence, which allows one to check the consistency of the method for different grid sizes. The second flow is the fully developed channel flow, which includes wall effects. The third case is the pulsed channel flow for which a considerable set of experimental data was produced by Binder and Kuény [5] and Tardu and Binder [15]. This flow case puts in light the lag effects appearing between the turbulent field and forcing. Given its non-equilibrium character, the latter flow is more relevant for our approach. These three flows constitute a first step for testing the split-spectrum model. More generally, the present approach is promised to cover a very wide range of applications, since unsteady turbulent flows are encountered in various situations of the industrial field and also since using coarse grids is an attractive economical method for practical methods of prediction.

First we present the basic equations of the large eddy simulation and the numerical method. A heuristic derivation of the new dissipation equation for subgrid scale turbulence introduces the basic idea of the method. A more detailed analytical development of the proposed model is then presented. The model is tested in simple fully turbulent flows with special attention to the influence of filter width on the results and also the wall influence. Then, the pulsed turbulent channel flow case gives an illustration of the potentials of the method in an unsteady situation, with comparisons to experiments and the testing of non-equilibrium effects. Future developments are suggested in the concluding remarks.

## 2 Basic equations

### *Filtered equations*

After a filtering operation is applied to the instantaneous Navier–Stokes equations, we obtain the following well-known equations of motion for LES:

$$\begin{cases} \frac{\partial \bar{U}_i}{\partial t} + \frac{\partial \bar{U}_i \bar{U}_j}{\partial x_j} = F_i - \frac{1}{\rho} \frac{\partial \bar{\pi}}{\partial x_i} - \frac{\partial \tau_{ij}}{\partial x_j} + \nu \nabla^2 \bar{U}_i \\ \frac{\partial \bar{U}_i}{\partial x_i} = 0 \end{cases} \quad (1)$$

in which  $\bar{U}_i$  is the filtered velocity,  $F_i$  is an external force and  $\tau_{ij}$  is the subgrid scale stress tensor. In the case of turbulent stress models using a subgrid scale viscosity hypothesis, the pressure  $\bar{\pi}$  will be referred to as the “pseudo-pressure” because it will also include the spherical part of the stress tensor. In this case the subgrid turbulent stresses are proportional to the filtered deformation of the flow field.

$$\tau_{ij} = -2\nu_{sgs} \bar{S}_{ij} \quad \text{with} \quad S_{ij} = \frac{1}{2} \left( \frac{\partial \bar{U}_i}{\partial x_j} + \frac{\partial \bar{U}_j}{\partial x_i} \right) \quad (2)$$

The present computations use a Gaussian filter in the periodic directions of the flow, with a smooth transition between resolved and unresolved scales. In the inhomogeneous directions, the filter produced by the grid discretization is used. The filter width  $\Delta_i$  is generally chosen to be twice the mesh spacing  $h_i$  in the corresponding direction ( $i$ ) (cf. Kwak et al. [26]). The filtering of the non-linear term in Eq. (1) is performed using this Gaussian filter. The reason for explicitly filtering the non-linear term is so that every term in the momentum equation has the same wavenumber content and the Leonard stresses are not neglected. Thus, in principle, the subgrid scale stress, a non-linear quantity, should also be explicitly filtered. In general, these equations are not exactly Galilean invariant (Vasilyev et al. [53]), but this point will not be discussed here.

### Numerical method

The filtered Navier–Stokes equations are solved using a hybrid Adams–Bashforth and Crank–Nicolson time scheme and the space discretization is based on Hermitian fourth order schemes in the inhomogeneous directions and Fourier pseudo-spectral developments in the homogeneous directions. This technique (Schiestel and Viazzo [43]; Viazzo and Schiestel [54]) proved to possess good conservation properties and numerical precision. However, this previous technique applied to the subgrid scale transport equations required a reduction of the time step to maintain stability. Therefore a different numerical time scheme based on first order accuracy approximation of derivatives and linearization of source terms was applied to the turbulence transport equations to keep a time step of the same order of magnitude as the one used in the Smagorinsky model calculation. The loss of accuracy being limited to the model itself, it has no serious drawbacks on the calculation of the resolved scales. A specific version has been developed for homogeneous turbulence using Fourier spectral developments in all three directions (for free decay of homogeneous turbulence). A description of the method is given in Appendix A.

### 3 An heuristic point of view for the $\varepsilon$ -equation in statistical modeling and subgrid modeling in LES

The subgrid scale model will be devised in order to be compatible with the two extreme limits that are the complete direct numerical simulation (DNS), and the one point full statistical modeling. This feature has to be dependent on the location of the cutoff produced by the filter. In the DNS, all the turbulent scales are resolved and the model is not active, whereas in the one point statistical modeling all the turbulent scales are modeled. Replaced in spectral space for homogeneous turbulence, this reasoning just indicates that the DNS is obtained when the filter cutoff  $\kappa_c$  goes to infinity, and full statistical modeling corresponds to the case of a vanishing cutoff.

We first give an interpretation of the usual  $\varepsilon$  equation in statistical modeling of homogeneous turbulence. Introducing the macro length scale of turbulence  $L$  allows to write:

$$\varepsilon = \alpha \frac{k^{3/2}}{L}, \quad (3)$$

where the coefficient  $\alpha$  is a dimensionless numerical constant.

It follows from Eq. (3) that:

$$\frac{d\varepsilon}{dt} = \frac{3\alpha}{2} \frac{k^{1/2}}{L} \frac{dk}{dt} - \alpha \frac{k^{3/2}}{L^2} \frac{dL}{dt}. \quad (4)$$

Using the kinetic energy equation:

$$\frac{dk}{dt} = P - \varepsilon,$$

where  $P$  is the production rate, leads to

$$\frac{d\varepsilon}{dt} = \frac{3}{2} \frac{(P - \varepsilon)}{T} - \frac{T}{L} \frac{dL}{dt} \frac{\varepsilon^2}{k} \quad (5)$$

with  $T = k/\varepsilon$  the time scale of the turbulence cascade.

The first term in the right hand side of (5) can be interpreted as the relaxation taking place in the spectral pipeline with the characteristic time of the cascade being equal to  $T$ . This term corresponds to the pure Kolmogoroff cascade. The second term shows that, in the absence of any external force, during free decay, the macroscale of turbulence increases, and consequently the dissipation rate is further decreased. The usual approximation in the  $k$ - $\varepsilon$  model consists of the hypothesis:

$$\frac{1}{\sqrt{k}} \frac{dL}{dt} = C_L \quad \text{or} \quad \frac{T}{L} \frac{dL}{dt} = C_T,$$

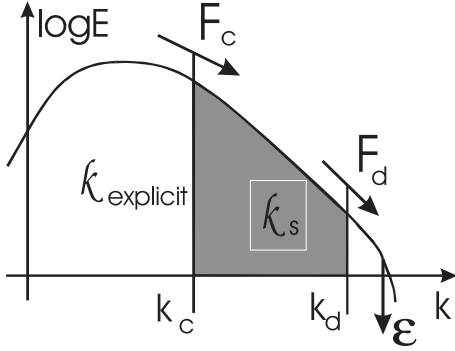


Fig. 1. Sketch of spectral partitioning for filtered turbulence

where  $C_L$  and  $C_T \cong 0.42$  are numerical constants. This approximation is equivalent to the standard  $k$ - $\varepsilon$  model for RANS closures:

$$\frac{d\varepsilon}{dt} = C_{\varepsilon 1} \frac{P\varepsilon}{k} - C_{\varepsilon 2} \frac{\varepsilon^2}{k} \quad \text{with} \quad C_{\varepsilon 1} = \frac{3}{2} \quad \text{and} \quad C_{\varepsilon 2} = \frac{3}{2} + \frac{T}{L} \frac{dL}{dt} (\cong 1.92). \quad (6)$$

Indeed, in unconstrained homogeneous turbulence the integral scale  $L$  increases.

In the case of subgrid scale modeling, the relaxation time scale  $T$  in the first term of (5) representing the pure Kolmogoroff transfer is replaced by  $k_s/\varepsilon$ , with  $k_s$  being the subgrid scale kinetic energy of turbulence. This relaxation time scale is thus smaller than previously, which is physically consistent because the spectral zone of cascade is reduced to  $[\kappa_c, \infty]$ . The production is also obviously replaced by the total energy flux  $F_C$  entering the subgrid zone (see Fig. 1). The second term in the right hand side of Eq. (5), however, does not change because physically the value of  $\varepsilon$  has not to be influenced by the choice of the cutoff. If one considers an equilibrium flow with  $P = F_C = \varepsilon$ , the first term vanishes and the second term must remain the same if we want  $\varepsilon$  to reach the same value as in the RANS  $\varepsilon$  equation. For instance, in channel flow this second term is balanced by the turbulent diffusion term. It can be written as  $\frac{T}{L} \frac{dL}{dt} \frac{k_s}{k} \frac{\varepsilon^2}{k_s}$  in order to derive the new  $\varepsilon$ -equation in the form:

$$\frac{d\varepsilon}{dt} = C_{1s} \frac{F_C \varepsilon}{k_s} - C_{2s} \frac{\varepsilon^2}{k_s} \quad \text{with} \quad C_{1s} = \frac{3}{2} \quad \text{and} \quad C_{2s} = \frac{3}{2} + \frac{T}{L} \frac{dL}{dt} \frac{k_s}{k}, \quad (7)$$

where  $F_C$  is the rate of energy entering the considered spectral zone, including production by the mean flow and the transfer through the splitting wavenumber, i.e., the energy flux transferred from the resolved scales to the subgrid scale non-resolved scales. It appears that the  $C_{2s}$  term goes to  $3/2$  when  $\kappa_c \rightarrow \infty (k_s \rightarrow 0)$  and goes to 1.92 when  $\kappa_c \rightarrow 0 (k_s \rightarrow k)$ .

Hereafter we present the detailed assessment of the  $k_s/k$  ratio using integration of an analytical spectrum function. Also, the subgrid scale transport equations for partial kinetic energy and dissipation rate are derived on more analytical grounds.

#### 4 Subgrid scale closure using partially integrated transport modeling (PITM)

We look now for a more detailed derivation of the method. The formulation of the transport equations for the turbulence energy  $k_s$  and for the dissipation rate relies on the multiscale approach (Schiestel [41]) applied to the splitted spectrum described in Fig. 1. The model for homogeneous turbulence is thus based on an integration in spectral space. The resulting characteristic length scale of the subgrid turbulence ( $\kappa > \kappa_c$  zone) will be given by  $L_{sgs} \approx \frac{k_s^{3/2}}{\varepsilon}$ .

In coarse meshes, indeed, the spectral cutoff can be located before the inertial spectral range and the calculation will indeed be a sort of VLES. If, in addition, the turbulence field is out of equilibrium, the space step size of the mesh will no longer be an acceptable estimate of the characteristic turbulence length scale for the subgrid scale turbulence. Such models that are able to separately calculate the subgrid turbulence are an appealing route in these cases.

In the following, we present an analytical derivation of the model using integration on spectral slices. The coefficients of the model are then calibrated in the particular case of the decay of homogeneous grid turbulence. Indeed, in this particular flow, the ratio  $k_s/k$  can be easily calculated from a given analytical spectrum shape. This allows the calibration of the  $C_{1s}$  and  $C_{2s}$  coefficients. The method can be easily extended to more general models such as non-linear models or stress transport models.

### Model for partial energies

The application of the multiscale approach is developed by choosing the spectral portioning sketched on Fig. 1. A first spectral portioning is made by introducing a cutoff  $\kappa_c$  located in the medium range of eddies and that figures out the filter operation in a large eddy simulation. The wavenumber  $\kappa_c$  is determined by the choice of the filter width. Secondly, as in the usual multiscale method (Schiestel [41]), a large wavenumber  $\kappa_d$  is introduced such that:

$$\kappa_d - \kappa_c = \xi \frac{\varepsilon}{k_s^{3/2}}. \quad (8)$$

The turbulence Reynolds number effect will not be considered at this stage, so that turbulence will be at high Reynolds number.

The constant  $\xi$  is chosen sufficiently large for  $\kappa_d$  to be located several logarithmic decades higher than  $\kappa_c$  at a point where the spectrum has strongly decreased and the energy located after  $\kappa_d$  will be considered as negligible. The energy contained in the  $[\kappa_c, \kappa_d]$  range is denoted  $k_s$ . Actually, this practice only implies that the transfer of energy through the wavenumber  $\kappa_d$  can be made equal to the dissipation rate, without dealing with infinite limits.

The partial turbulence kinetic equation related to the range  $[\kappa_c, \infty]$  is

$$\frac{dk_s}{dt} = \mathcal{F}_c - \mathcal{E}_c \frac{d\kappa_c}{dt} - \varepsilon. \quad (9)$$

This relation states that the net transfer  $F_c = \mathcal{F}_c - \mathcal{E}_c \frac{d\kappa_c}{dt}$  through the cutoff  $\kappa_c$  is the sum of the spectral flux at this wavenumber and the rate of energy exchange due to the variation of the splitting wavenumber. We can write a similar equation,  $\varepsilon = \mathcal{F}_d - \mathcal{E}_d \frac{d\kappa_d}{dt}$ , for the transfer occurring at the wavenumber  $\kappa_d$ , taking into account that the energy located after  $\kappa_d$  is negligible and thus  $\mathcal{F}_d = \varepsilon$ .

Using both of these relations in Eq. (8), gives after taking the derivative:

$$\frac{d}{dt} \left( \xi \frac{\varepsilon}{k_s^{3/2}} \right) = \frac{\mathcal{F}_d - \varepsilon}{\mathcal{E}_d} - \frac{\mathcal{F}_c - F_c}{\mathcal{E}_c} \quad (10)$$

and then, using (9) and (10):

$$\frac{d\varepsilon}{dt} = \frac{3}{2} \frac{\varepsilon}{k_s} (F - \varepsilon) - \frac{k_s}{(\kappa_d - \kappa_c) \mathcal{E}_d} \left[ \left( 1 - \frac{\mathcal{F}_d}{\varepsilon} \right) - \frac{F_c}{\varepsilon} \frac{\mathcal{E}_d}{\mathcal{E}_c} \left( 1 - \frac{\mathcal{F}_c}{F_c} \right) \right] \frac{\varepsilon^2}{k_s}. \quad (11)$$

The second term inside the large brackets is supposed to be negligible because  $\mathcal{E}_d \ll \mathcal{E}_c$  and also because the grid size is almost fixed or slowly variable (in the case of variable step size of the grid), implying that  $F_c \cong \mathcal{F}_c$ . So,

$$\frac{d\varepsilon}{dt} = \underbrace{\frac{3}{2}}_{C_{s1}} \frac{\varepsilon}{k_s} F - \underbrace{\left[ \frac{3}{2} - \frac{k_s}{\kappa_d \mathcal{E}_d} \left( \frac{\mathcal{F}_d}{\varepsilon} - 1 \right) \right]}_{C_{s2}} \frac{\varepsilon^2}{k_s}. \quad (12)$$

When  $\kappa_c$  goes to zero the usual RANS  $\varepsilon$  equation is recovered with  $k_s \rightarrow k$  and  $C_{2s} \rightarrow C_{\varepsilon 2} = \frac{3}{2} - \frac{k}{\kappa_d \mathcal{E}_d} \left( \frac{\mathcal{F}_d}{\varepsilon} - 1 \right)$ . By comparing the expressions of  $C_{\varepsilon 2}$  (previous relation) and  $C_{2s}$  (Eq. (12)), we can deduce the values of the coefficients in the subgrid scale  $\varepsilon$  equation:

$$C_{s1} = \frac{3}{2} \quad \text{and} \quad C_{s2} = \frac{3}{2} + \frac{k_s}{k} \left( C_{\varepsilon 2} - \frac{3}{2} \right). \quad (13)$$

These relations highlight the dependency of the coefficient  $C_{s2}$  on the ratio  $k_s/k$ , explained earlier in the heuristic presentation of the method (cf. Eq. (7)). This dependence allows one to link the large-scale part of the spectrum to the modeled subgrid-scale part.

### *Calibration on decay of grid turbulence*

The particular case of the decay of turbulence behind a grid in the initial period of decay is considered for estimating the shape spectrum ratio  $k_s/k$  and then to calibrate the model coefficients. It is usually admitted that the energy spectrum at very low wavenumbers (Lesieur [29]) behaves like:

$$\mathcal{E} \approx C\kappa^\mu \quad \text{for } \kappa \rightarrow 0,$$

whereas in the inertial range at high wavenumbers, the Kolmogoroff spectrum has to be recovered:

$$\mathcal{E} \approx \chi\epsilon^{2/3}\kappa^{-5/3} \quad \text{for large } \kappa.$$

Some authors (Aupoix [2]) have developed modeling from piecewise integration of an energy spectrum approximated by the two previous laws joined by a knee. Smoother approximations have been proposed by Von Karman (cf. Hinze [20]) that also have the nice property of leading to easily integrable functions. For convenience, we shall use here a function of this kind, that has the correct behavior both at small wavenumbers and in the inertial range:

$$\mathcal{E}(\kappa) = \frac{\chi\epsilon^{2/3}\kappa^\mu}{\left[\left(\frac{\chi\epsilon^{2/3}}{C}\right)^{\frac{m-1}{m+\mu}} + \kappa^{m-1}\right]^{\frac{m+\mu}{m-1}}} \quad \text{with } m = 5/3, \quad (14)$$

where  $\chi$  is the Kolmogorov constant.

Using partial integration (cf. Appendix B), the ratio  $k_s/k$  can be calculated analytically:

$$\frac{k_s}{k} = 1 - \left( \frac{\eta_c^{2/3}}{\frac{\chi}{1+\mu} + \eta_c^{2/3}} \right)^{\frac{3}{2}(\mu+1)} \quad (15)$$

with  $\eta_c = \frac{\kappa_c}{\kappa_{\text{ref}}}$  and  $\kappa_{\text{ref}} = \epsilon/k^{3/2}$ .

This result is then inserted in (13) for coefficient  $C_{s2}$ .

The important feature of this approximation is that:

$$\frac{k_s}{k} \approx \frac{3}{2}\chi\eta_c^{-2/3} \quad \text{when } \eta_c \rightarrow \infty. \quad (16)$$

This behavior is in agreement with the equations derived in Rubinstein and Zhou [37, 38]. In their work, these authors propose to derive the  $\epsilon$  equation from integration of analytical models. The connection with the multiscale approach is developed in Rubinstein and Zhou [38].

Also, when  $\eta_c \rightarrow 0$ , it is verified that  $k_s \rightarrow k$ , corresponding to full statistical modeling.

So, in principle the analytic formula (15) allows one to specify the variations of the  $C_{s2}$  coefficient in the subgrid scale  $\epsilon$ -equation (Eq. (12)). The analytical expression for  $k_s/k$  allows the coefficient  $C_{s2}$  to vary in compliance with the grid mesh size. So, the variation of  $C_{s2}$  acts as a dynamical parameter that determines the asymptotic spectral shape in which the turbulence relaxes (regardless of the other processes of production and diffusion).

### Practical formulation of the PITM model

A dimensionless cutoff wavenumber can be defined by:

$$\mathcal{N}_c = \kappa_c \mathcal{L} , \quad (17)$$

where  $\mathcal{L}$  is the characteristic length scale of the whole spectrum. In the general case, the characteristic length scale  $\mathcal{L}$  can be evaluated according to the previous definition:

$$\mathcal{L} \approx \frac{(k_{\text{simul}} + k_s)^{3/2}}{\varepsilon} . \quad (18)$$

The cutoff wavenumber  $\kappa_c$  will be approximated by the filter width of the LES:

$$\kappa_c = \pi \left( \frac{1}{\Delta x \Delta y \Delta z} \right)^{1/3} . \quad (19)$$

This choice does not account for the anisotropy of the grid. When the grid is very elongated, like in the near wall region, useful approximation formulas have been introduced (Scotti, Meneveau and Lilly [45]) to account for grid anisotropies. However, we preferred to keep the model as simple as possible. Such improvements can be incorporated in future work.

For simplicity, Eqs. (13) and (15) can be replaced by a simpler function that retains the correct asymptotic behavior:

$$C_{s1} = 1.5 \quad \text{and} \quad C_{s2} = 1.5 + 0.42 \frac{1}{1 + \beta \mathcal{N}_c^{2/3}} . \quad (20)$$

We again emphasize the fact that coefficient  $C_{s2}$  varies in compliance with spatial step size variations. It is interesting to remark that the difference:

$$C_{s2} - C_{s1} = \frac{0.42}{1 + \beta \mathcal{N}_c^{2/3}} \quad (21)$$

varies from 0.42 for full statistical modeling down to zero when DNS is approached and looks like the indicator of the relative proportion of the spectrum that is modeled. Indeed, when  $C_{s2} = C_{s1}$  the turbulence cannot be sustained. In the opposite limit of full statistical modeling,  $k_{sgs} \rightarrow k$  and the usual  $k$ - $\varepsilon$  model is exactly retrieved with  $C_{s2} = 1.92$  and  $C_{s1} = 1.50$ .

The parameter  $\beta$  is a constant of order unity determined from Eq. (16) that gives  $\beta \approx 2/3\chi \approx 0.44$ . The practical value has been calibrated in the case of homogeneous decaying turbulence and plane channel flow. The best results have been obtained for  $\beta = 0.375$ , a value that is very close to the theoretical estimate.

### Subgrid scale eddy viscosity

The subgrid scale turbulent stresses are obtained in the present model by an eddy viscosity hypothesis. The subgrid turbulence diffusion can be estimated according to the Heisenberg hypothesis (cf. Hinze [20]):

$$\nu_{sgs} = C_\kappa \int_\kappa^\infty \kappa^{-3/2} \mathcal{E}(\kappa)^{1/2} d\kappa . \quad (22)$$

Using the Kolmogoroff spectrum  $\mathcal{E}(\kappa) = \chi \varepsilon^{2/3} \kappa^{-5/3}$ , one finds:

$$\nu_{sgs} = \frac{3}{4} C_\kappa \chi^{1/2} \varepsilon^{1/3} \kappa^{-4/3} \quad \text{or} \quad \nu_{sgs} = \frac{3}{4} C_\kappa \chi^{1/2} \frac{k^2}{\varepsilon} \eta_c^{-4/3} \quad (23)$$

and remarking that  $\frac{k_s}{k} \approx \frac{3}{2} \chi \eta_c^{-2/3}$ , this implies:

$$\nu_{sgs} = \frac{1}{3} C_\kappa \chi^{-3/2} \frac{k_s^2}{\varepsilon} . \quad (24)$$

In order to satisfy the necessary compatibility with the asymptotic value in the  $k$ - $\varepsilon$  full statistical modeling, we are led to choose:

$$v_{sgs} = C_\mu \frac{k_s^2}{\varepsilon} \quad \text{with} \quad C_\mu = 0.09. \quad (25)$$

The use of Eq. (23) implies that the cutoff is near the inertial zone. For more generality, a variable  $C_\mu$  would probably be useful, but we have not considered this issue in the present paper.

In practice, hypothesis (25) may generate too much fluctuation in viscosity and some averaging is necessary by using  $v_{sgs} = C_\mu L_{sgs} \sqrt{k_s}$  with an averaged characteristic scale  $L_{sgs} = \left( \frac{k_s^3}{\varepsilon} \right)^{1/2}$ . In such a case, the statistical averaging is made in homogeneous directions and/or in time.

### *Inhomogeneous flows*

In non-homogeneous flows the turbulent diffusion terms have to be taken into account in the partial kinetic energy equation and the dissipation equation:

$$\frac{dk_s}{dt} = F_c - \varepsilon + \mathcal{D}_{ksgs} \quad (26)$$

$$\frac{d\varepsilon}{dt} = C_{1s} \frac{F_c P}{k_s} - C_{2s} \frac{\varepsilon^2}{k_s} + \mathcal{D}_{\varepsilon sgs} \quad (27)$$

with a gradient diffusion hypothesis:

$$\mathcal{D}_{ksgs} = \left( \frac{v_{sgs}}{\sigma_{ksgs}} (k_s)_{,j} \right)_{,j} \quad \text{and} \quad \mathcal{D}_{\varepsilon sgs} = \left( \frac{v_{sgs}}{\sigma_{\varepsilon sgs}} \varepsilon_{,j} \right)_{,j}. \quad (28)$$

In order to compare with the standard full  $k$ - $\varepsilon$  model, the previous equations are averaged in the mean:

$$\frac{\partial \langle k_s \rangle}{\partial t} + \langle U_j \rangle \langle k_s \rangle_{,j} = \langle F_c \rangle - \langle \varepsilon \rangle + \left( \frac{v_{sgs}}{\sigma_{ksgs}} \langle k_s \rangle_{,j} \right)_{,j} - \langle u'_{(e)j} k' \rangle_{,j} \quad (29)$$

$$\frac{\partial \langle \varepsilon \rangle}{\partial t} + \langle U_j \rangle \langle \varepsilon \rangle_{,j} = C_{1s} \frac{\langle F_c \rangle \langle P \rangle}{\langle k_s \rangle} - C_{2s} \frac{\langle \varepsilon \rangle^2}{\langle k_s \rangle} + \left( \frac{v_{sgs}}{\sigma_{\varepsilon sgs}} \langle \varepsilon \rangle_{,j} \right)_{,j} - \langle u'_{(e)j} \varepsilon' \rangle_{,j} \quad (30)$$

with:  $U_j = \underbrace{\langle U_j \rangle + u'_{(e)j}}_{\bar{U}_j} + u'_{(i)j}$  and  $k_s = \langle k_s \rangle + k'$  where  $u'_{(e)j}$  and  $u'_{(i)j}$  denote respectively the resolved part

and the modeled part of the fluctuating velocity.

The diffusion terms verify the property:  $\langle u'_j \phi' \rangle = \langle u'_{(e)j} \phi' \rangle + \langle u'_{(i)j} \phi' \rangle$ .

We have also used the approximations  $\langle F_c P \rangle \approx \langle F_c \rangle \langle P \rangle$  and  $\langle \varepsilon^2 \rangle \approx \langle \varepsilon \rangle^2$ .

These equations clearly exhibit the diffusion term  $\langle u'_{(e)j} k' \rangle_{,j}$  and  $\langle u'_{(e)j} \varepsilon' \rangle_{,j}$  due to the resolved fluctuations of turbulence whereas  $\langle u'_{(i)j} k' \rangle_{,j} = - \left( \frac{v_{sgs}}{\sigma_{ksgs}} \langle k_s \rangle_{,j} \right)_{,j}$  and  $\langle u'_{(i)j} \varepsilon' \rangle_{,j} = - \left( \frac{v_{sgs}}{\sigma_{\varepsilon sgs}} \langle \varepsilon \rangle_{,j} \right)_{,j}$  are the modeled terms of diffusion due to non-resolved microturbulence.

Written in the particular case of the logarithmic boundary layer near a wall, the  $\varepsilon$ -equation then gives:

$$(C_{s2} - C_{s1}) \frac{\langle \varepsilon \rangle^2}{\langle k_s \rangle} = C_\mu \frac{k^2}{\sigma_{\varepsilon sgs}} \left( \frac{\langle \varepsilon \rangle_{,j}}{\langle \varepsilon \rangle} \right)_{,j} \quad (31)$$

in which the diffusion term includes the resolved and the non-resolved parts.

Taking into account  $(C_{s2} - C_{s1}) \frac{k}{k_s} = C_{\varepsilon 2} - C_{\varepsilon 1}$  and  $\left( \frac{\langle \varepsilon \rangle_{,j}}{\langle \varepsilon \rangle} \right)_{,j} = \frac{1}{z^2}$ , we find that the value  $\sigma_{\varepsilon sgs} = 1.3$  has to be the same as in the standard  $k$ - $\varepsilon$  model. For compatibility with the standard  $k$ - $\varepsilon$  model we also have  $\sigma_{ksgs} = 1.0$ .

In confined wall flows, the relation (18) can be replaced by  $\mathcal{L}_w = Kz$ , where  $z$  is the distance from the nearest wall and  $K$  is the Von Karman constant. The correspondence with Eq. (20) is obtained by considering the logarithmic law of the wall with:

$$k \approx a u_*^2 \quad \text{and} \quad \varepsilon = \frac{u_*^3}{Kz} \quad \text{with} \quad a = 3.3$$

and using the previous definitions, one easily finds:

$$\mathcal{L} = \frac{k^{3/2}}{\varepsilon} = a^{3/2} Kz = a^{3/2} \mathcal{L}_w$$

and then  $\mathcal{N}_c = a^{3/2} \kappa_c \mathcal{L}_w$ .

Therefore Eq. (20) can be written equivalently:

$$C_{s2} = 1.5 + 0.42 \frac{1}{1 + \beta_w \left[ \left( \frac{1}{\Delta x \Delta y \Delta z} \right)^{1/3} \mathcal{L}_w \right]^{2/3}} \quad \text{with} \quad \beta_w = a\pi^{2/3} \beta. \quad (32)$$

### Low Reynolds number extension

The final model is then complemented by low Reynolds number extensions that are important very near a wall. In this respect, a transposition of the Jones and Launder [24]  $k$ - $\varepsilon$  model is made, for implementing lower order terms in the pseudo-dissipation equation. The coefficients that are functions of the turbulence Reynolds number are derived from the Launder and Sharma [28] variant:

$$\begin{aligned} \frac{\partial \tilde{\varepsilon}}{\partial t} + \bar{U}_j \frac{\partial \tilde{\varepsilon}}{\partial x_j} = & C_{1s} \frac{\tilde{\varepsilon}}{k_s} v_{sgs} \frac{\partial \bar{U}_i}{\partial x_j} \left( \frac{\partial \bar{U}_i}{\partial x_j} + \frac{\partial \bar{U}_j}{\partial x_i} \right) + \frac{\partial}{\partial x_j} \left( \frac{v_{sgs}}{1.3} \frac{\partial \tilde{\varepsilon}}{\partial x_j} \right) + v \frac{\partial^2 \tilde{\varepsilon}}{\partial x_j \partial x_j} \\ & - (C_{1s} + (C_{2s} - C_{1s}) f_{\varepsilon_{sgs}}) \frac{\tilde{\varepsilon}^2}{k_s} + 2v v_{sgs} \left( \frac{\partial^2 \bar{U}_j}{\partial x_m \partial x_p} \right)^2 \end{aligned} \quad (33)$$

and  $\varepsilon = \tilde{\varepsilon} + 2v \left( \frac{\partial \sqrt{k_s}}{\partial x_j} \right)^2$  for dissipation rate, with  $f_{\varepsilon_{sgs}} = 1.0 - \exp(-R_{sgs}^2)$ ,  $v_{sgs} = 0.09 \exp\left(\frac{-3.4}{(1+R_{sgs}/50)^2}\right) \frac{k_s^2}{\tilde{\varepsilon}}$ ,  $R_{sgs} = \frac{k_s^2}{\tilde{\varepsilon}}$ .

The  $f_{\varepsilon_{sgs}}$  term has been chosen such that when  $\kappa_c \rightarrow 0$  and  $k_s \rightarrow k$ , the usual  $k$ - $\varepsilon$  model of Launder and Sharma is approximately recovered. For this, the two corresponding terms are identified:

$$\left[ C_{s1} + (C_{s2} - C_{s1}) f_{\varepsilon_{sgs}} \right] \frac{\varepsilon^2}{k} = C_{\varepsilon 2} \left[ 1 - 0.3 \exp(-R_{sgs}^2) \right] \frac{\varepsilon^2}{k}$$

giving:

$$f_{\varepsilon_{sgs}} = 1 - \frac{0.3 C_{\varepsilon 2}}{C_{\varepsilon 2} - C_{\varepsilon 1}} \exp(-R_{sgs}^2) \approx 1 - \exp(-R_{sgs}^2). \quad (34)$$

### Limiting behaviors

The limit of the model when  $\kappa_c \rightarrow 0$  is obviously identical to the standard  $k$ - $\varepsilon$  model with full statistical modeling.

However, we must mention that if the cutoff wavenumber  $\kappa_c$  is very small (smaller than the wavenumber corresponding to the maximum of the energy spectrum), then the use of a pure eddy viscosity model becomes questionable and more general models including backscatter may be necessary.

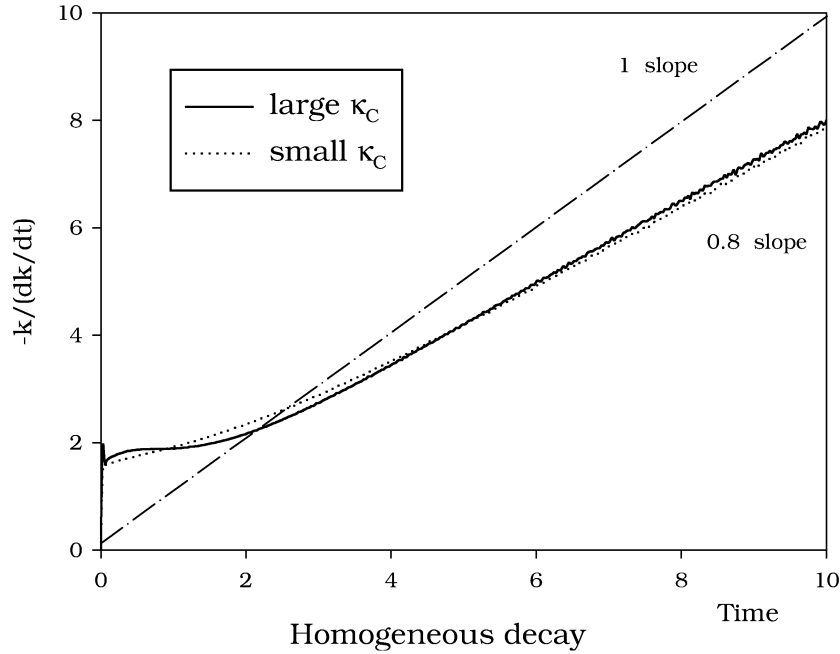


**Fig. 2.** Decay rate of homogeneous isotropic turbulence, LES with two-equation subgrid scale model, effect of filter width

When  $\kappa_c \rightarrow \infty$ , the behavior of the model is more subtle. In this case, the ratio  $k_s/k$  goes to zero and the limit  $C_{s2} \rightarrow C_{s1}$  in Eq. (12) corresponds to a pure Kolmogoroff behavior. Indeed, in the general case, changes in  $\varepsilon$  occur when imbalance is present between  $F_C$  and  $\varepsilon$ . But, in an equilibrium situation  $F_C = \varepsilon$ , and  $\varepsilon$  does not change and consequently  $C_{s2} = C_{s1}$ . This reasoning is made for infinite Reynolds numbers. In real cases however, the subgrid scale Reynolds number  $Re_{sgs}$  goes to zero when  $\kappa$  approaches the Kolmogoroff scales and then, to get  $k_s = 0$ , a low Reynolds number version of the model is necessary. To enforce the model to give a true DNS in this limit, it would be possible to introduce a viscous cutoff by taking  $C_\mu = 0$  if  $\kappa_\eta/\kappa_c < 1$  where  $\kappa_\eta$  is the Kolmogoroff wavenumber  $\varepsilon^{1/4}/\nu^{3/4}$  (but it is useless in practice, because the model is obviously not intended to run as a DNS).

## 5 Preliminary tests in fully developed turbulence

### *Decay of homogeneous turbulence*

The decay of homogeneous isotropic turbulence is the simplest test case to check the correct behavior of the model. A specific spectral Fourier version of the code (Schiestel [40]) has been used in this case. An analytical homogeneous pseudo-random field has been generated as initial condition with a prescribed energy spectrum defined by:

$$\begin{aligned} \mathcal{E} &\approx C\kappa^{1.4} & \text{for } \kappa \leq \kappa_0, \\ \mathcal{E} &\approx \chi\varepsilon^{2/3}\kappa^{-5/3} & \text{for } \kappa \geq \kappa_0. \end{aligned} \quad (35)$$

The maximum of the spectrum is obtained for  $\kappa_0$  defined by the continuity of the two expressions in Eq. (35). Both the resolved part of the initial energy and the subgrid part are determined from Eq. (35).

Keeping the same number of grid points  $80^3$ , the filter width was varied. Two values have been considered, a large cutoff  $\kappa_c = \kappa_{\max}$  and a small cutoff  $\kappa_c = \kappa_{\max}/2$ , where  $\kappa_{\max}$  is the maximum wavenumber of the grid. The practical choice of the cutoff is such that  $\kappa_{\max} \approx 4\kappa_0$ . In the present case the general definition  $\mathcal{N}_c = \kappa_c \frac{(k_{\text{simul}} + k_s)^{3/2}}{\varepsilon}$  is retained for the dimensionless cutoff wavenumber involved in the  $C_{s2}$  coefficient. The value of the parameter  $\beta = 0.375$  established in Sect. 4 has been found to give satisfactory results. Figure 2 shows the decay of kinetic energy. All quantities have been normalized on the initial total kinetic energy and the initial value of the length scale  $\mathcal{L}_0 = \frac{\pi}{\kappa_0}$  defined on the initial energy spectrum. As is found in experimental grid turbulence in the initial period (Comte-Bellot and Corrsin [6, 7]), the decay law is faster than the

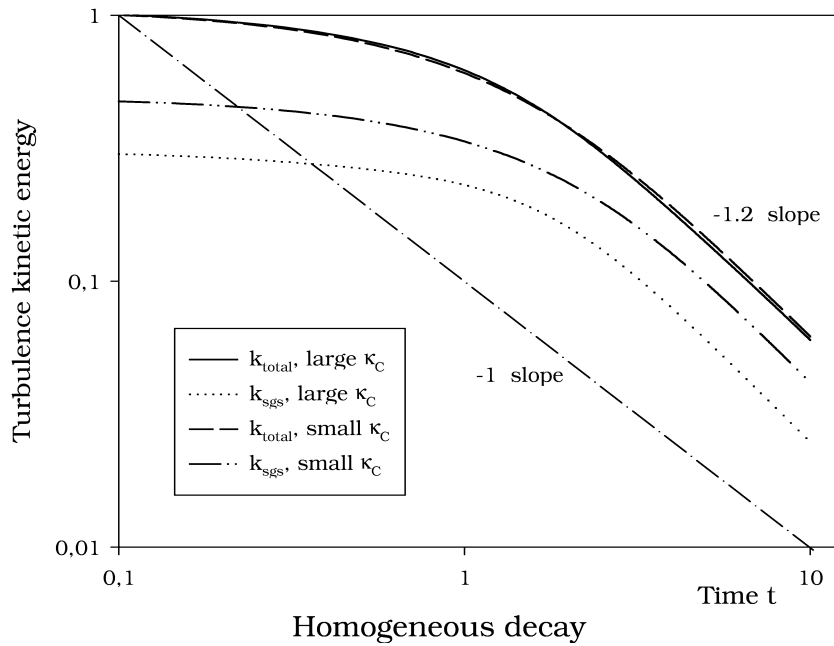


**Fig. 3.** Decay rate of homogeneous isotropic turbulence, LES with two-equation subgrid scale model

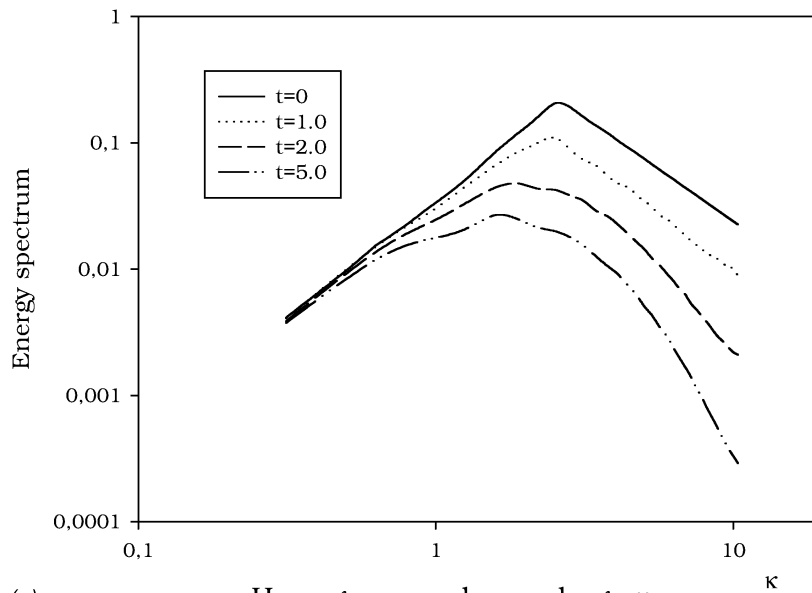
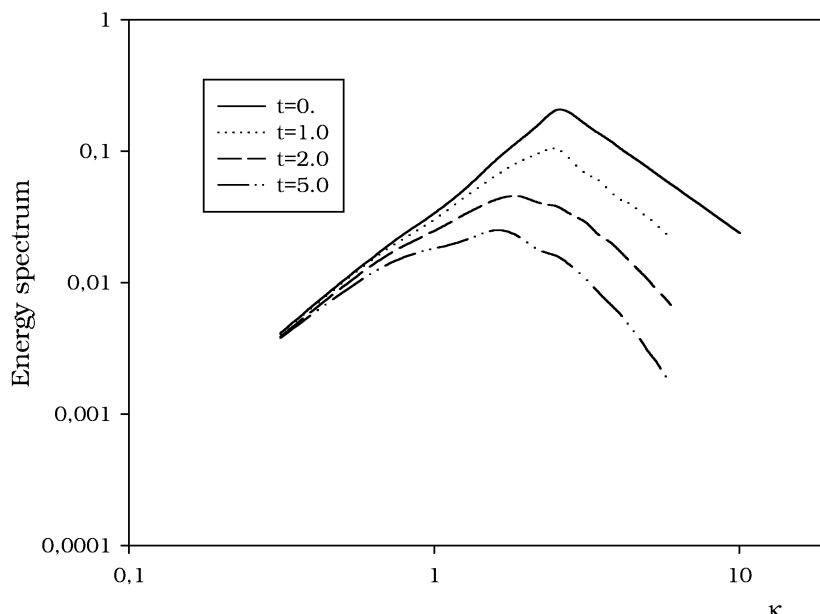
$\alpha t^{-1}$  power law. As mentioned before, the time variable  $t$  is normalized using  $\frac{\mathcal{L}_0}{\sqrt{k_{\text{initial}}}}$  in Figs. 2 to 5. The turbulence Reynolds number is about 800 in the initial conditions and decays down to 250 for  $t = 5$  and 190 for  $t = 10$ . In order to obtain the law of decay, the time scale  $\tau = k/(-dk/dt)$  is plotted versus time in Fig. 2. The slope is then the inverse of the decay exponent found to be nearly 1.2. Figure 3, which uses the more usual log-log plot confirms this value of decay rate. This latter figure also shows that changing the value of  $\kappa_c$  does not modify the evolution of the total kinetic energy. However, as expected, the ratio of the resolved part to the modeled part is strongly different. Figure 4a and b confirm that the evolution of the energy spectrum of the resolved field for both values of the filter width remain consistent during decay and so the low wavenumber part of the spectrum is found to be independent of the cutoff location, showing the good behavior of the model when the filter width is varied.

Figure 5 shows the evolution of the characteristic length scale  $k_s^{3/2}/\varepsilon$  of the subgrid turbulence for the two filter widths. In this quasi-equilibrium situation (slow decay), the model gives a characteristic length that is almost constant with an asymptotic value that is very close to the scale given by the filter itself, equal to  $\pi/\kappa_c$  and that takes the values 0.4 and 0.8, respectively, for the sharp filter and for the large filter.

#### *Standard fully developed turbulent channel flow*

The model has first been tested on the classical case of fully developed turbulent channel flow that corresponds to quasi-equilibrium turbulence. For this case, the low Reynolds number extensions of the model presented above (Sect. 4) have been introduced in the computations. The same value of the parameter  $\beta = 0.375$  (or  $\beta_w = 2.5$ ) has been used throughout all applications.

The channel flow has been simulated for a Reynolds number (the Reynolds number is based on center line velocity and channel half width) equal to 13 800 with a relatively coarse mesh composed of  $32 \times 64 \times 62$  points in the domain with box sizes ( $L_x = 2\pi\delta$ ,  $L_y = \pi\delta$ ,  $L_z = 2\delta$ ). The calculation has been made with imposed mean pressure gradient corresponding to  $\text{Re}_\tau = 640$  as in the LES of Moin and Kim [31]. The statistically steady state is approximately reached after a total time of about integration  $Tu_\tau/\delta = 5$ , corresponding to more than ten thousand time steps. The LES calculation of Moin and Kim [31] has been extended to DNS for approximately the same Reynolds number by Moser et al. [32] ( $\text{Re}_\tau = 590$ ). The mean velocity profile (Fig. 6) is compared to the DNS result of Moser et al. [32] and to the usual log law. Compared to the DNS of the Moser et al. [32] the two-equation model prediction has a wall friction coefficient that is approximately 10% higher, probably partly because the statistic is not perfectly attained

(a) Homogeneous decay, large  $\kappa_C$ (b) Homogeneous decay, small  $\kappa_C$ 

**Fig. 4.** Decay of homogeneous isotropic turbulence, LES with two-equation subgrid scale model, energy spectrum, (a) large cutoff, (b) small cutoff

(imposed pressure gradient calculations have very slow statistical convergence (see Deschamps [14]). The main discrepancy in the mean velocity profile is a departure from the log law. Several reasons can be put forward to explain this discrepancy. The main reason involves the well-known deficiencies of the statistical low Reynolds number  $k$ - $\varepsilon$  model as discussed in the paper of Sarkar and So [39]. In particular, the paper of Patel et al. [34] shows that the Launder and Sharma model leads to some overshoot above the usual log law. This type of weakness can surely be cured by a better choice of the low Reynolds number functions in the  $k$ - $\varepsilon$  model and will not be considered in the present paper. It is worth mentioning here that our approach used by Hanjalic et al. [19] to derive their “seamless model” for LES/RANS calculations, but making use of the  $k$ - $\varepsilon$  model of Abe et al. [1] instead of the  $k$ - $\varepsilon$  model of Launder and Sharma to approximate the wall effects, considerably improves the velocity profile. This shows that the low Reynolds number terms can explain some of the discrepancies found in Fig. 6 and that a better choice of low Reynolds number terms requires some more testing that is beyond the scope of the present pa-

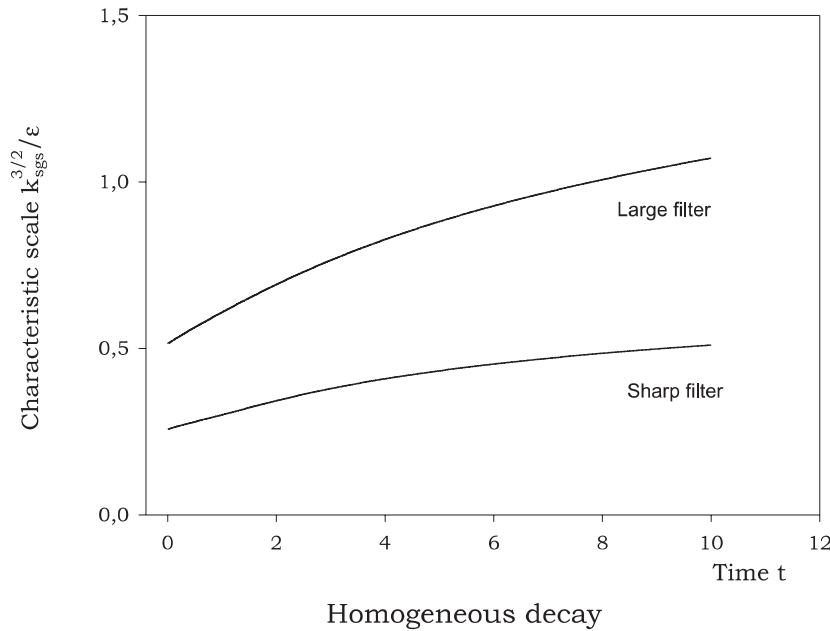


**Fig. 5.** Decay of homogeneous isotropic turbulence, LES with two-equation subgrid scale model, characteristic scale of subgrid turbulence

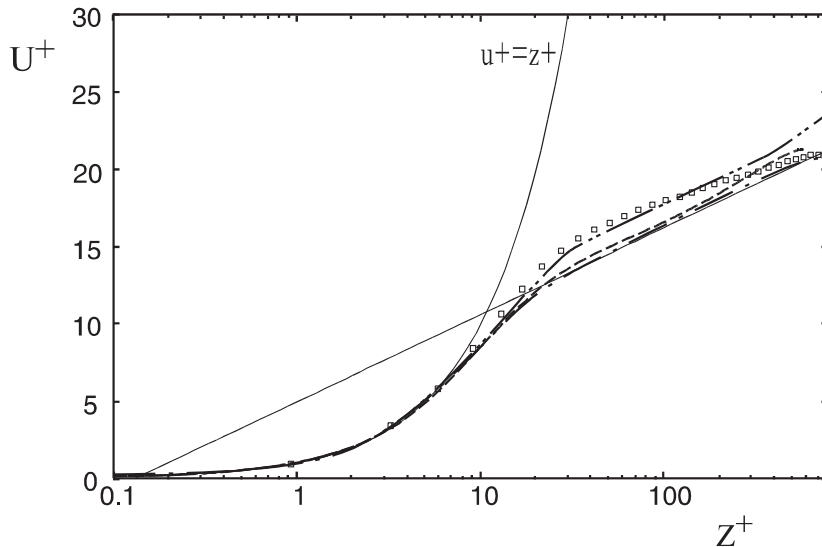


**Fig. 6.** Mean velocity profiles in plane channel flow. ( $\square$ ) present two-equation subgrid scale model ( $32 \times 64 \times 62$ ); (---) DNS, Moser et al. [32]  $Re_\tau = 590$ ; (- · - · -) Moin and Kim [31], ( $64 \times 63 \times 128$ ),  $Re = 13800$ ; (- - - -) Launder and Sharma  $k-\epsilon$  RANS model (from Patel et al. [34])

per. The Abe model seems an interesting possibility but other versions of the  $k$ -epsilon may be candidate as well.

Another point is related to the relative coarseness of the grid, which can also lead to discrepancies in the outer layer of the velocity profile (cf. Piomelli et al. [36]). Hybrid methods or DES also hardly produce an accurate logarithmic slope and some improvements are still desirable (cf. Nikitin et al. [33]). Recently, it has been shown that the inclusion of backscatter effect at the interface RANS/LES region improves the velocity profile (Piomelli et al. [35]).

When the turbulent field is considered, the profiles of the mean turbulence intensities (Figs. 7 to 9) and the total turbulent shear stress (sum of the resolved and the modeled shear stresses) given in Fig. 10 obtained from the two-equation subgrid scale model are in satisfactory agreement with known experimental data at the same Reynolds number (Hussain and Reynolds [23]; Wei and Willmarth [55]) and with the DNS

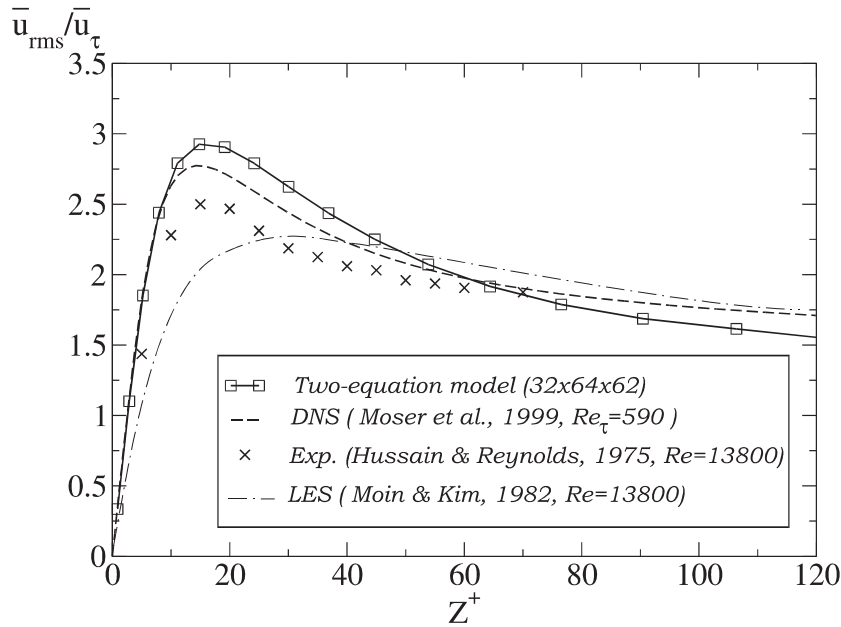


**Fig. 7.** Mean longitudinal turbulence intensity profiles in plane channel flow. ( $\square$ ) two-equation model ( $32 \times 64 \times 62$ ); (---) Moser et al. ([32],  $Re_\tau = 590$ ); (-·-·-) Moin and Kim ([31],  $Re = 13800$ ); ( $\times$ ) Hussain and Reynolds experiment [23] (1975,  $Re = 13800$ )

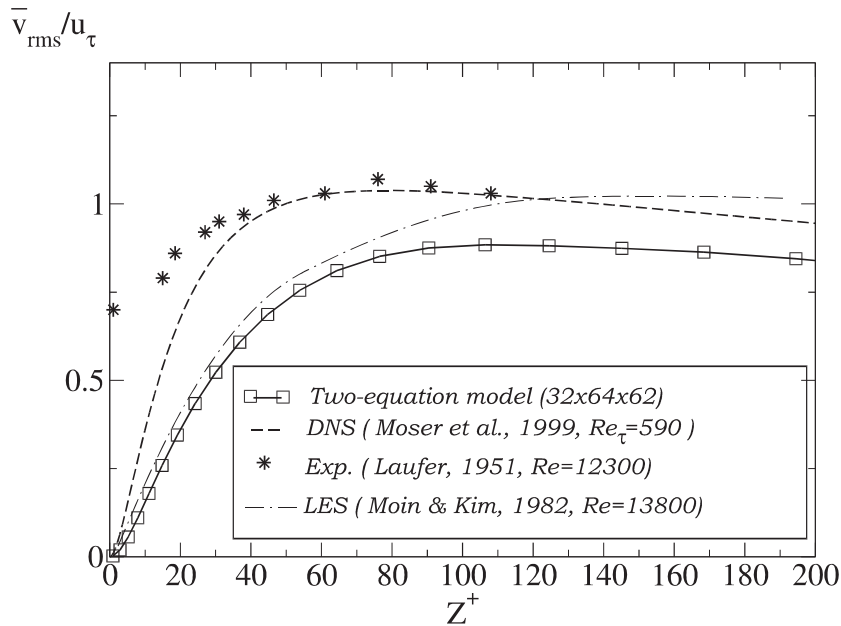


**Fig. 8.** Mean normal turbulence intensity profiles in plane channel flow. ( $\square$ ) two-equation model ( $32 \times 64 \times 62$ ); (---) Moser et al. ([32],  $Re_\tau = 590$ ); (-·-·-) Moin and Kim ([31],  $Re = 13800$ ); (\*) Laufer experiment (1951,  $Re = 12300$  based on channel half-width and maximum mean velocity)

of Moser et al. [32] at a nearby Reynolds number (Fig. 7). The peak of the turbulence energy in the production zone is located around  $z^+ = 14$  like in most experiments. One can note on Fig. 10 that the contribution of the model to the turbulent shear stress is dominant in the near wall region up to the distance  $z^+ = 20$ , so that the approximation of low Reynolds number effects mentioned earlier are influential in this region of the flow.

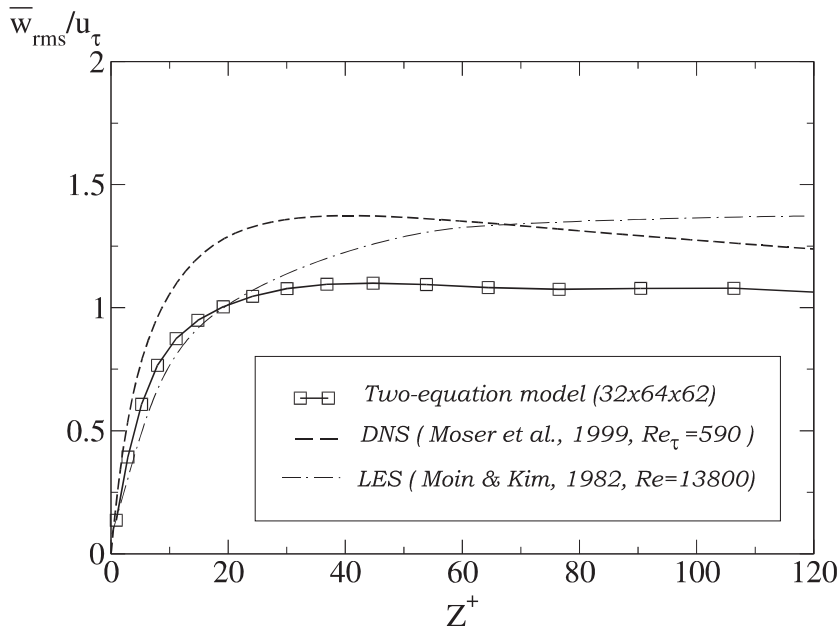


**Fig. 9.** Mean transverse turbulence intensity profiles in plane channel flow. ( $\square$ ) two-equation model ( $32 \times 64 \times 62$ ); (---) Moser et al. ([32],  $Re_\tau = 590$ ); (-·-·-) Moin and Kim (1982,  $Re = 13800$ )

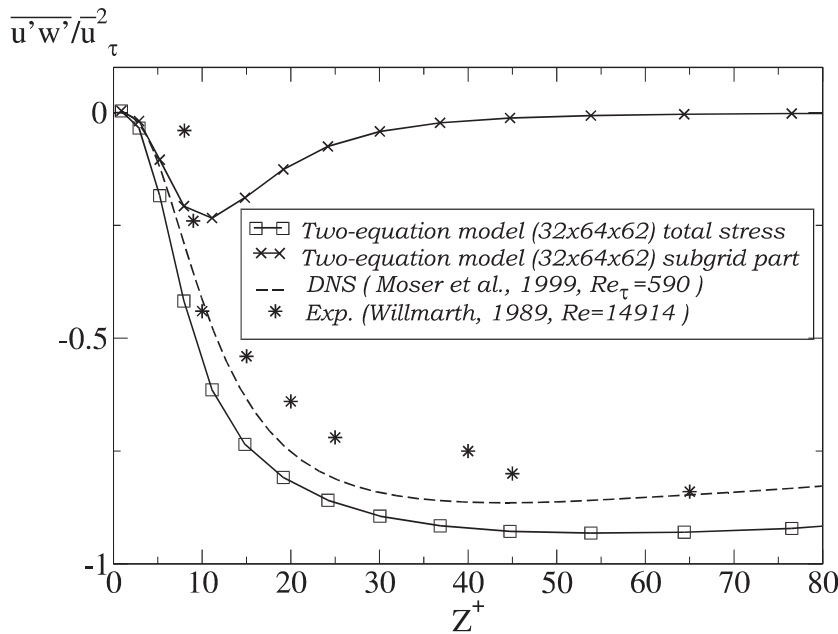


**Fig. 10.** Mean turbulent shear stress profiles in plane channel flow, total shear stress. ( $\square$ ) two-equation model ( $32 \times 64 \times 62$ ); (---) Moser et al. ([32],  $Re_\tau = 590$ ); (\*) Willmarth experiment (1989,  $Re = 14914$ ); (x) modeled subgrid scale part of shear stress

We have shown that the transport subgrid scale model has a general consistent behavior in channel flow regardless some discrepancies found in the mean velocity profile that could be probably cured by revising the choice of low Reynolds number form of the model coefficients. However, these first results are very encouraging to further pursue the study of non-zonal RANS-LES formulation developed here. The results obtained by Hanjalic et al. [19], using our concept of variable  $C_{2s}$  coefficient, are interesting in this respect and show appropriate velocity profiles in the channel flow.

The turbulent channel flow includes wall effects but it is still a quasi-turbulent equilibrium flow. The main objective of the present approach addresses non-equilibrium turbulence. It is then interesting to test the new model in such a situation. This is illustrated by the application to turbulent pulsed channel flow, which is now considered.

## 6 Study of unsteady oscillatory turbulent flows in the mean

To illustrate some of the potentials of the new model, the application to unsteady turbulent flow with periodic forcing is considered (Dejoan [10]; Dejoan and Schiestel [11]; Dejoan and Schiestel [12]). A considerable experimental work on the pulsed channel flow done by Binder and Kuény [5], Tardu and Binder [15] and Tardu, Binder et al. [51] is available. The experimental results exhibit important lag effects appearing between the modulation of the turbulent stresses and the forcing, these lag effects depending on the frequency of the imposed oscillation. The periodic forcing is produced by a longitudinal sinusoidal mean pressure gradient (Fig. 11). These experiments highlight that the response of the turbulent flow to the forcing can be characterized by

three frequency regimes: a quasi-steady regime, a relaxation regime and a high frequency regime (see below). Such a flow has also been studied by Scotti et al. [46] who used large eddy simulations with the dynamic model of Germano. These authors report numerical results for several frequency regimes of periodic forcing that are in good agreement with experiments. They have considered, however, different amplitude values of the forcing.

The rationale of the present study is to show that the split spectrum model is able to deal with non-equilibrium turbulence. Therefore, we have chosen a frequency regime for which strong lag effects are observed between the turbulent field and the forcing. This regime corresponds to the relaxation regime described in more details hereafter. In order to highlight the ability of the proposed model to tackle the unsteady character of the turbulence in pulsed channel flow, we present in addition to the comparisons with the experiments, comparisons with the well-known Smagorinsky subgrid scale model, which relies implicitly on an equilibrium hypothesis (cf. Appendix C).

### *Term decomposition*

The analysis of unsteady periodic flows is based on a formalism using a four-terms decomposition:

$$q = \langle q \rangle + \tilde{q} + q'_{\text{exp}} + q'_{\text{imp}}. \quad (36)$$

The statistical mean value is identified as the phase average and can be in its turn, split into a time mean value and a periodic oscillation. The fluctuating turbulent part is composed of a resolved part, which is simulated, and a non-resolved part, which is modeled.

### *Pulsed channel flow characteristics*

The periodic forcing (Fig. 11) is produced by a longitudinal sinusoidal mean pressure gradient in the channel  $F_x = -(1 + A_F \sin(\omega t))$ .

Turbulent pulsed flows have been largely studied in boundary layers and channel flows, and their behavior is indeed very complex. In particular, the research work of Binder and Kuény [5], Tardu and Binder [15], Tardu et al. [51], Tardu [49] and Feng et al. [15], has put in light the governing parameter for periodic wall flows that is the dimensionless Stokes parameter defined by  $l_s^+ = l_s u_* / \nu$  with  $l_s = \sqrt{2\nu/\omega}$ . In terms of the

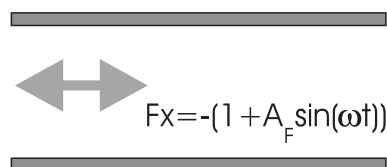


**Fig. 11.** Sketch of pulsed channel flow

Strouhal number, the characteristic parameter is  $\omega^+ = \omega v / u_\tau^2$ , which is directly linked to the dimensionless Stokes length parameter by using the relation  $\omega^+ = 2 / l_s^{+2}$ . The Stokes length  $l_s$  can be interpreted as the distance from the wall at which the oscillation diffuses. Then, when the frequency is higher, the wall layer influenced by the oscillation becomes more and more confined near the wall, and much of the flow in the channel core is a piston flow.

We have chosen for the present numerical application the value  $l_s^+ = 12.9$  belonging to an intermediate frequency range, in which a strong interaction is expected between the imposed oscillation frequency and the turbulence scales themselves (cf. Tardu et al. [51] and Binder et al. [4]). Keeping in mind that the contribution of the model is dominant up to the distance  $z^+ = 20$  from the wall and that in this near-wall region the velocity profile behaves properly (cf. Fig. 6), the frequency value  $l_s^+ = 12.9$  turns out to be a reasonable choice for testing the model in the pulsed channel flow. The amplitude is chosen to be weak, the ratio  $A_{\bar{u}_c} / U_c$  being of order of 5%.

The numerical simulation has been carried on for the two-equation model and the Smagorinsky model on a grid mesh identical to the one used in the fully developed turbulent channel flow (cf. Appendix C for the Smagorinsky model formulation).

#### *Analysis of the response of the flow to the imposed oscillation*

In the experiment it is generally reported that the time mean flow is not affected by forcing. Indeed, the time mean value for the velocity or longitudinal turbulence intensity are comparable to those prevailing in the corresponding steady flow. Identical observations have been found in our computation when comparing the time mean quantities of the pulsed channel flow with the time mean quantities of the fully developed channel flow.

However, if we consider the phase averages, the effect of the oscillation is obvious. To gain more insight in the analysis of the results, the phase averages are transposed in the Fourier space and the amplitude and phase of the first Fourier mode is considered.

Practically, good statistical convergence has been obtained by considering about 24 periods in time for phase averaging.

#### *Modulation of mean velocities*

The amplitude and phase shift of the fundamental Fourier mode of the oscillating mean velocity versus distance from the wall are drawn on Figs. 12 and 13. They are found to be weakly dependent on the model and both are close to the experimental data. The variation in amplitude values is not far from the Stokes solution with a steep gradient near the wall, and a plateau in the bulk flow. The phase shift variation exhibits the decrease in response time scale of the velocity when it becomes further from the wall.

#### *Modulation of the turbulent field*

The evolution of the amplitude of the fundamental Fourier mode of the normal longitudinal turbulent stress with the normal direction is shown in Fig. 14. In the experiment of Tardu et al., the amplitude is similar in shape to the turbulence intensity itself, with a peak region in the region  $z^+ = 12$  and a progressive decay afterwards. Figure 14 shows that the two-equation model is successful in predicting the experimental peak in amplitude near the wall, but predicts a too high amplitude modulation. On the contrary, the Smagorinsky model seems to provide a better quantitative amplitude but does not predict the near-wall peak and the amplitude decay is also not well-reproduced far from the wall. In the range of forcing amplitude  $0.05 < a_{\bar{u}} < 0.6$  (see Binder et al. [5] and Tardu et al. [51]), the maximum amplitude  $A_{uu}^{1/2} / u_\tau$  is observed to vary from 0.2 to 3.5. However, in all the cases, the profiles are very similar in shape and exhibit a near wall peak similar to the steady turbulent wall flow (see Fig. 7). The amplitude of the forcing used in the work of Scotti and Piomelli [46] is considerably larger than the one used in the present calculation, this is the main reason why the comparisons between various experiments and calculations are difficult in absolute value. The work of Tardu et al. shows that the amplitude of the modulation of turbulence intensity is very dependant on the  $l_s^+$  parameter and also of the amplitude of the forcing, however the shape of the curve of the amplitude of modulation remain almost the same in all cases. The type of normalization used in Fig. 14 is suggested in Tardu

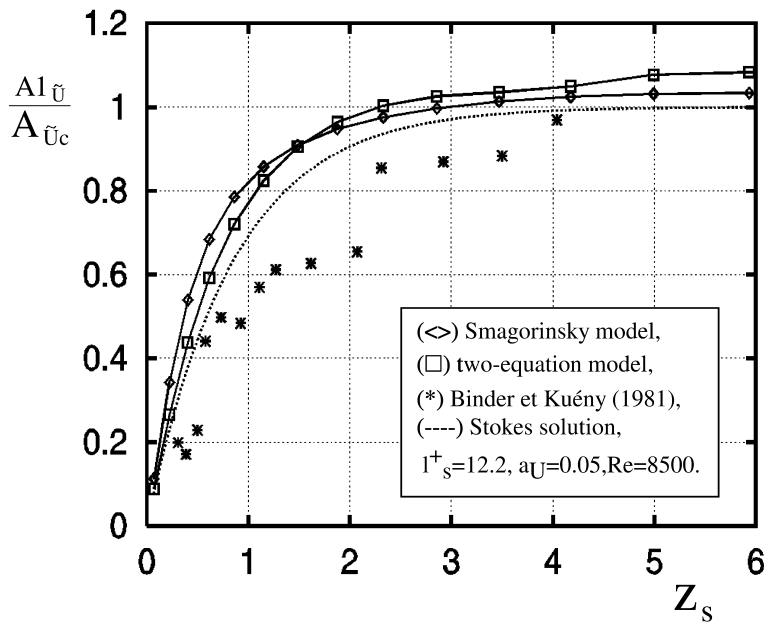


**Fig. 12.** Amplitude of the fundamental mode of the oscillating velocity deviation from axial velocity. ( $\diamond$ ) Smagorinsky model ( $32 \times 64 \times 62$ ); ( $\square$ ) split-spectrum model ( $32 \times 64 \times 62$ ); (\*) Binder and Kuény experiment [5],  $l_s^+ = 12.2$ ,  $a_U = 0.05$ ,  $Re = 8500$ ; (.....) Stokes solution

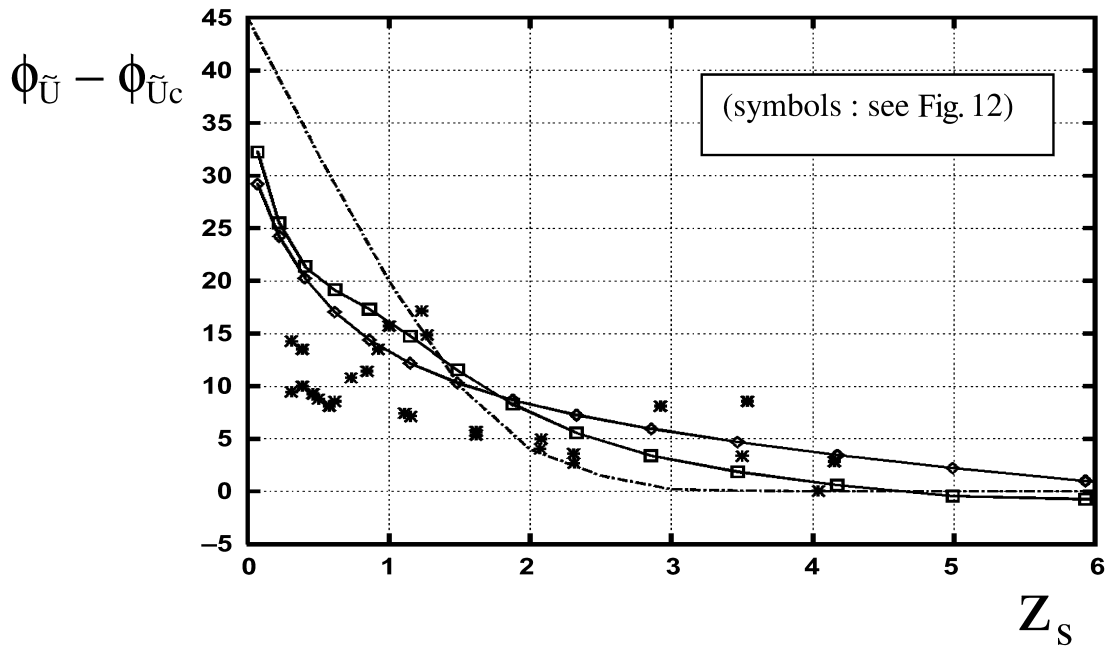


**Fig. 13.** Phase shift of the fundamental mode of the oscillating velocity deviation from axial velocity (symbol definitions as in Fig. 12)

et al. [51], it allows one to keep all the plots within a limited scale of representation. It is worth mentioning that the amplitude of forcing in the Binder et al. [5] experiment is very low, and the authors in their publication indicate that for this reason the accuracy of measurement of the amplitude of the modulation is not really sufficient and that these measurements must be considered in a qualitative sense. So Fig. 14 shows that, in spite of important scatter in the absolute values of amplitudes (due to different values of the forcing amplitude), the shape of the curve found using the present model is satisfactory.

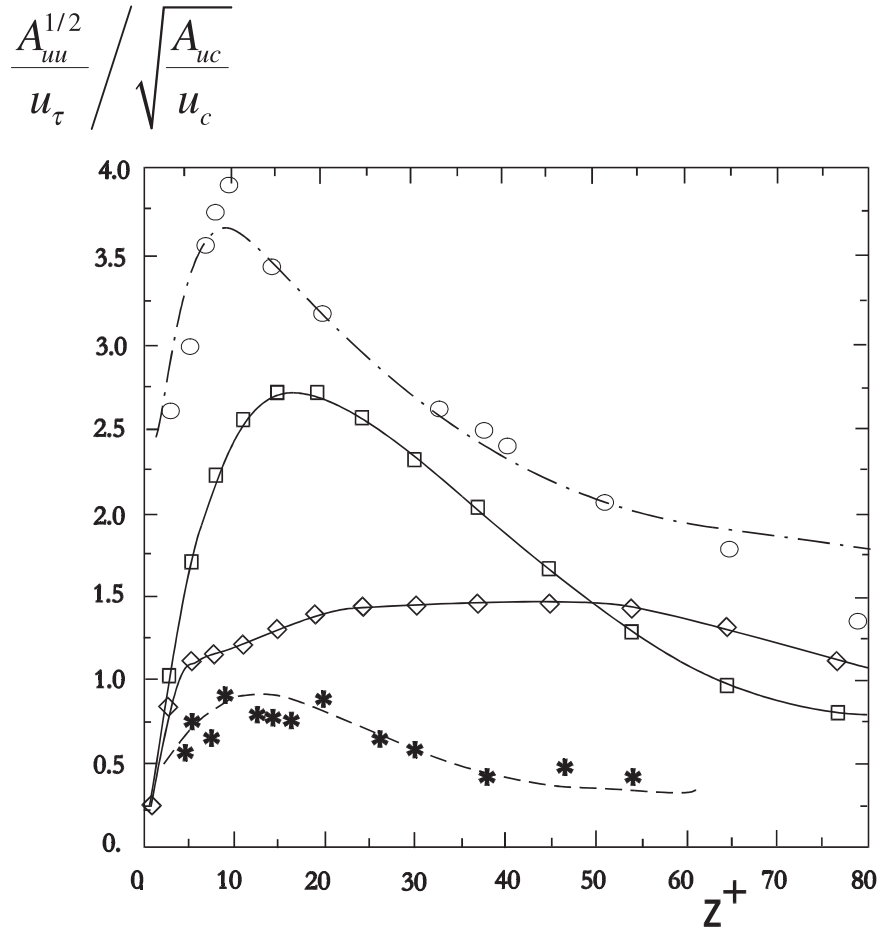


**Fig. 14.** Relative amplitude of the fundamental mode of the longitudinal turbulence intensity. ( $\diamond$ ) Smagorinsky model ( $32 \times 64 \times 62$ ); ( $\square$ ) two-equation model ( $32 \times 64 \times 62$ ); ( $-\cdot-\cdot-$ ) numerical simulation, Scotti and Piomelli [46],  $l_s^+ = 14$ ,  $a_{\bar{v}} = 0.64$ ; ( $* \cdots \cdots$ ) from Binder and Kuény experiment [5] with experimental fitted curve,  $l_s^+ = 12.2$ ,  $a_{\bar{v}} = 0.05$ ,  $Re = 8500$ ; ( $\circ$ ) Tardu et al. [51],  $l_s^+ = 16$ ,  $a_{\bar{v}} = 0.64$

These discrepancies may be also related to the tendency of the statistical  $k-\varepsilon$  model of overestimating the effect of forcing observed by Scotti and Piomelli [47], who have tested several URANS models, and among them, the  $k-\varepsilon$  model, in a pulsating flow.

Considering the phase shift reported in Fig. 15, the time delay of the longitudinal turbulent intensity to the forcing is far better predicted by the two-equation model than by the Smagorinsky model. The time response of the turbulent field can also be represented in terms of time delay, which characterizes the diffusion speed of the modulation (cf. Fig. 16) if we use the following relation of Tardu et al. [51]:

$$\Delta t^+ = \frac{1}{2}(\phi_{u'u'} - \phi_{\bar{v}c})l_s^2, \quad (37)$$

where the phase shift is given in radians.

The experiments of Tardu et al. have shown that in the range  $8.1 < l_s^+ < 34.$ , and for all values of the forcing amplitude considered, the variations of the time delay versus distance from the wall, satisfy a linear law of decay such that  $dz^+/d(\Delta t^+) \approx 0.4$  for  $z^+ > 30$ . The equivalent relation, recast in terms of phase lag, becomes  $d(\phi_{u'u'} - \phi_{\bar{v}c})/dz^+ = 2.5\omega^+$  and is also found to be in good agreement with the two-equation model predictions. The split-spectrum approach shows to be successful in predicting of phase shifts by an account of time lag effects whereas the Smagorinsky model fails. The phase shift is not very sensitive to the amplitude of forcing and the comparison with the results of Scotti et al. [46] is satisfactory.

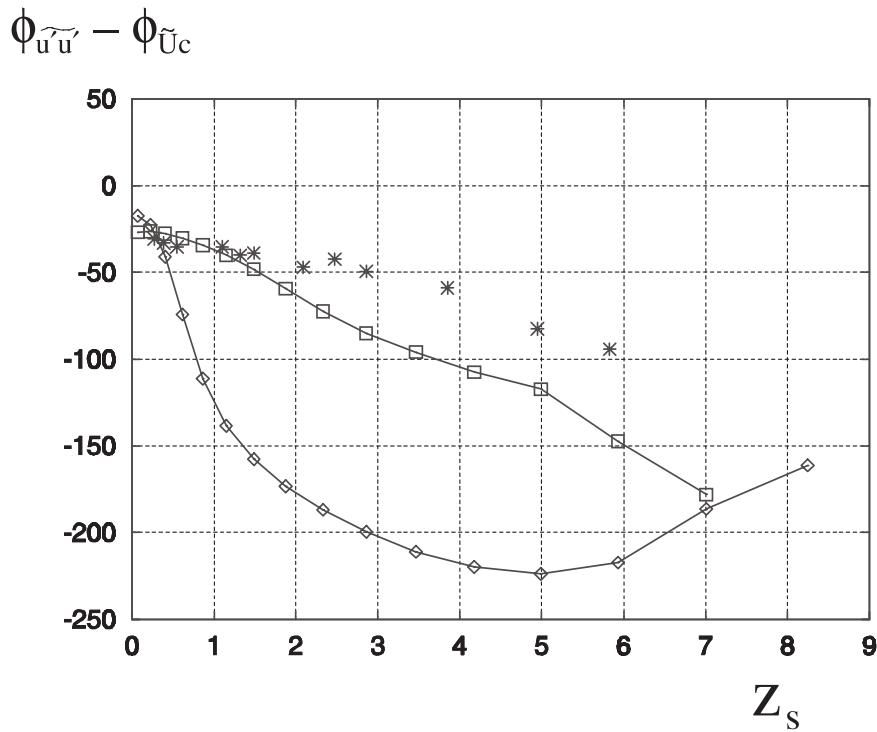


**Fig. 15.** Phase shift of the fundamental mode of the longitudinal turbulence intensity. ( $\diamond$ ) Smagorinsky model ( $32 \times 64 \times 62$ ); ( $\square$ ) split-spectrum model ( $32 \times 64 \times 62$ ); (\*) Binder and Kuény experiment [5],  $l_s^+ = 12.2$ ,  $a_{\tilde{u}} = 0.05$ ,  $Re = 8500$

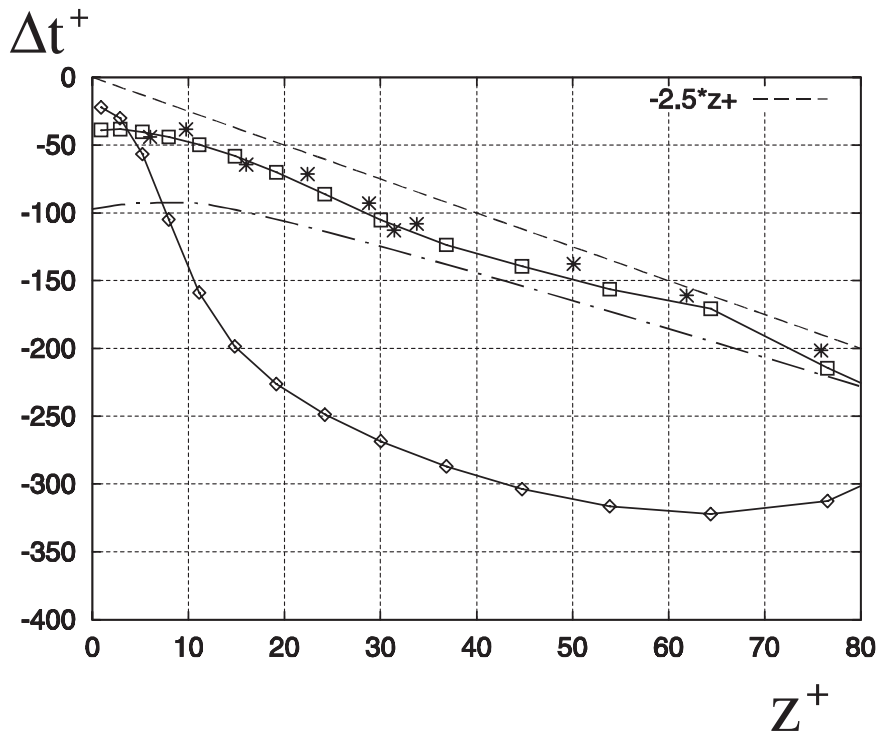


**Fig. 16.** Dimensionless diffusion time lag of the fundamental mode of the longitudinal turbulence intensity. ( $\diamond$ ) Smagorinsky model ( $32 \times 64 \times 62$ ); ( $\square$ ) split-spectrum model ( $32 \times 64 \times 62$ ); (- - -) numerical simulation, Scotti and Piomelli [46],  $l_s^+ = 14$ ,  $a_{\tilde{u}} = 0.64$ ; (\*) Tardu, Binder and Blackwelder experiment [51],  $l_s^+ = 12.2$ ,  $a_{\tilde{u}} = 0.2$ ,  $Re = 8500$ ; (- · - ·)  $d(\phi_{\tilde{u}\tilde{u}} - \phi_{\tilde{u}_c})/dz^+ = 2.5\omega^+$  law

## 7 Concluding remarks

A new subgrid scale model based on partial integrated transport equations has been presented. The general formalism is based on the spectral portioning concept and is here applied in order to derive a two-transport-equations model that includes one equation for the subgrid partial kinetic energy and another equation for the dissipation energy decay rate. The main novel feature of the proposed model is the new form of the  $\varepsilon$ -equation applicable to LES. This latter equation looks like the  $\varepsilon$ -equation in the well-known  $k$ - $\varepsilon$  RANS model but the coefficients are now functions of the cutoff location. The form of the equations is consistent with the extreme limits that are on one hand direct numerical simulation and on the other hand full statistical modeling. This type of model is devised for LES with coarse grids, in which the modeled part of the spectrum goes below the inertial range, and for more general models than models based on equilibrium hypothesis are necessary. This is particularly useful when dealing with non-equilibrium flows such as perturbed or unsteady flows. Indeed, the present method allows one to develop turbulence models that describe only a slice or a part of the turbulence spectrum, which can account for departure from equilibrium. The method has been presented for a two-equation model for partial energy and dissipation but it can be readily extended to more complex models including Reynolds stress transport models. The transport model brings new concepts in the development of non-zonal hybrid models that bridge the LES approach and the RANS approach in a continuous way.

The application carried out on the decay of homogeneous turbulence showed that the split-spectrum model behaves in a consistent way regarding the variation of the filter width and conservation of the total turbulence energy. The application for fully turbulent channel flow and unsteady turbulent flows in pulsed channel flow has put in light the interesting potentials of the method. However, the results obtained for the turbulent steady channel flow indicate that further developments related to the description of wall effects are desirable. This includes the use of different low Reynolds number coefficients (referring to a different low Reynolds number RANS model). In this sense, the results recently obtained by Hanjalic et al. using a seamless model, derived from our approach but using different wall effects approximations, for a RANS/LES calculation of a fully developed channel flow are quite encouraging. They show improvements on the velocity profile and also illustrate the flexibility of our formalism to include new improved low Reynolds number RANS models. Also, a thorough study of low Reynolds number effects should be undertaken. Interesting results have been obtained in unsteady channel flow with periodic forcing, in particular for phase shift effects. In this pulsed channel flow case however, the model is observed to overpredict the amplitude of the oscillating turbulent field, however, the near wall peak of the amplitude is well predicted and the temporal response closely follows the measurements.

The set of results presented here is promising and encouraging to pursue further developments. Extended applications of the method to various types of flows and various filter widths have to be undertaken to illustrate the capabilities of the method in more general situations. For strongly anisotropic turbulent flows, subgrid scale stress transport equations based on second moment statistical closures should be also considered. This is however beyond the scope of the present work, whose main purpose was to establish the foundation of a general formalism for PITM for LES calculations.

*Acknowledgment.* The calculations were carried out on the supercomputers at the IDRIS computer center in Paris and is gratefully acknowledged.

## Appendix A

### *Numerical method for non-homogeneous flows*

The filtered momentum equations are solved on shifted grids using a hybrid numerical method based on Hermitian fourth order schemes and pseudo-spectral Fourier developments (Schiestel and Viazzo [43]). In the non-homogeneous directions, the mesh is strongly refined near the walls. The time advancement is based on a hybrid Adams–Bashforth and Crank–Nicolson scheme and the pressure-velocity coupling is achieved efficiently by iteratively solving a simplified pressure correction equation.

For solving the subgrid scale turbulence equation of the transport model, a first order time scheme was introduced for the  $k_s$  and  $\varepsilon_{sgs}$  equations, because of stability requirements. The precision loss concerns only the modeled equations.

The spatial derivatives are calculated as previously, using centered Hermitian schemes. The source terms are linearized for iterative solution.

### *Numerical method for homogeneous flows*

A specific version of the simulation code has been developed for homogeneous flows. All three directions in space are solved using spectral Fourier series. In this case, the pressure can be easily eliminated in the momentum equations and uniform non-shifted grids can be used. The time scheme is also an Adams–Bashforth and Crank–Nicolson scheme.

## **Appendix B**

### *Model calibration on an analytical spectrum of homogeneous decaying turbulence*

An analytical spectrum approximation similar to that proposed by Von Karman (cf. Hinze [20]) has been used:

$$\mathcal{E}(\kappa) = \frac{\chi \varepsilon^{2/3} \kappa^\mu}{\left[ \left( \frac{\chi \varepsilon^{2/3}}{C} \right)^{\frac{m-1}{m+\mu}} + \kappa^{m-1} \right]^{\frac{m+\mu}{m-1}}} \quad (\text{B1})$$

with  $m = 5/3$ , and  $\chi = 1.5$  (Kolmogorov constant).

The hypothesis of permanence of big eddies is taken into account through the fact that  $C$  is assumed to be constant. Integration of the spectrum gives:

$$k = \int_0^\infty \mathcal{E}(\kappa) \cdot d\kappa = \frac{1}{\mu + 1} \left( C^{\frac{2/3}{\mu+1}} \chi \varepsilon^{2/3} \right)^{3 \frac{\mu+1}{3\mu+5}} \quad (\text{B2})$$

whereas the  $k$ -equation reduces to  $\frac{dk}{dt} = -\varepsilon$ .

It can be easily deduced from the previous equations that:

$$\frac{d\varepsilon}{dt} = - \underbrace{\left( \frac{3\mu + 5}{2(\mu + 1)} \right)}_{C_{\varepsilon 2}} \frac{\varepsilon^2}{k}. \quad (\text{B3})$$

This result is the same as the Aupoix [26] result using the “knee” spectrum. The usual value  $C_{\varepsilon 2} = 1.92$  is obtained for  $\mu = 1.4$ . This decay law corresponds in fact to a self-similar decay in which the spectrum varies in scale but not in shape. If we introduce a non-dimensional wavenumber  $\eta = \frac{\kappa}{\kappa_{\text{ref}}}$ , with  $\kappa_{\text{ref}} = \varepsilon/k^{3/2}$ , the energy spectrum is then  $\mathcal{E}(\kappa) = \frac{k}{\kappa_{\text{ref}}} \mathcal{E}^*(\eta)$  with:

$$\mathcal{E}^*(\eta) = \frac{\chi \eta^\mu}{\left( \frac{\chi}{1+\mu} + \eta^{2/3} \right)^{\frac{3\mu+5}{2}}} \quad \text{and} \quad \mathcal{H}^*(\eta) = \int_0^\eta \mathcal{E}^* d\eta = \left( \frac{\chi \eta^{-2/3}}{1+\mu} + 1 \right)^{-\frac{3}{2}(\mu+1)}. \quad (\text{B4})$$

The determination of the coefficient  $C_{s2}$  can be made by evaluating the ratio  $k_s/k$ :

$$\frac{k_s}{k} = 1 - \mathcal{H}^*(\eta_c) \quad (\text{B5})$$

and consequently:

$$\frac{k_s}{k} = 1 - \left( \frac{\eta_c^{2/3}}{\frac{\chi}{1+\mu} + \eta_c^{2/3}} \right)^{\frac{3}{2}(\mu+1)} \quad (\text{B6})$$

(note that in the inertial range the partial kinetic energy reduces to  $k_s = \int_{\kappa_c}^{+\infty} \chi \varepsilon^{2/3} \kappa^{-5/3} d\kappa$ ).

## Appendix C

### *Smagorinsky model, low Reynolds number extension*

For comparison purpose, each flow case has been calculated using the classical Smagorinsky model. Its low Reynolds extension used here is briefly recalled. The viscosity in Eq. (2) is defined by:

$$\nu_{sgs} = (C_s l)^2 \sqrt{2 \cdot \bar{S}_{ij} \bar{S}_{ij}} \quad \text{for } z \geq z_C \quad (\text{C1})$$

$$\nu_{sgs} = C_2 \frac{l^4}{\nu} (2 \cdot \bar{S}_{ij} \bar{S}_{ij}) \quad \text{for } z \leq z_C \quad (\text{C2})$$

with:

$$l = [\Pi \min(\Delta_m, l^*)]^{1/3} \quad (\text{C3})$$

$$l^* = 0.1\delta/C_s \quad \text{for } z \geq 0.1\delta/\kappa \quad (\text{C4})$$

$$l^* = \kappa z/C_s \quad \text{for } z \leq 0.1\delta/\kappa \quad (\text{C5})$$

and the numerical constants:

$$C_s = 0.2, \quad C_s = C_s^2 \nu / 27 \kappa u_\tau, \quad \kappa = 0.41 \quad (\text{Karman constant}).$$

In Eq. (B3), the filter width in the ( $m$ ) direction is denoted  $\Delta_m$ ,  $\delta$  is the distance between the two walls, and  $z$  is the wall distance. This model cannot take into account any historical effect.

## References

1. Abe, K., Kondoh, T., Nagano, Y.: A new turbulence model for predicting fluid flow and heat transfer in separating and reattaching flows-I. Flow field calculations. *Int. J. Heat Mass Transf.* **37**, 139–151 (1994)
2. Aupoix, B.: *Application de modèles dans l'espace spectral à d'autres niveaux de fermeture en turbulence homogène*. Dissertation, Université Lyon I (1987)
3. Batten, P., Goldberg, U.C., Palaniswamy, S., Chakravarthy, S.R.: Hybrid RANS/LES: Spatial resolution and energy-transfer issues. In: *Proc. Symp. on Turbulence and Shear Flow Phenomena, Second Int. Symp.*, KTH, Stockholm, vol. 2, pp. 159–164 (2001)
4. Binder, G., Tardu, S., Vezin, P.: Cycle modulation of Reynolds stresses and length scales in pulsed channel flow. *Proc. Roy. Soc. Lond. A* **451**, 121–139 (1995)
5. Binder, G., Kuény, J.L.: Measurements of the periodic oscillations near the wall in unsteady turbulent channel flow. In: Michel R., Cousteix J., Houdeville R. (eds.) *Unsteady Turbulent Shear Flows*. IUTAM Symp. Springer Berlin Heidelberg New York, pp. 100–109 (1981)
6. Comte-Bellot, G., Corrsin, S.: The use of a contraction to improve the isotropy of grid generated turbulence. *J. Fluid Mech.* **25**(4), 657–682 (1966)
7. Comte-Bellot, G., Corrsin, S.: Simple Eulerian time correlation of full and narrow-band velocity signals in grid-generated 'isotropic' turbulence. *J. Fluid Mech.* **48**, 273–337 (1971)
8. Davidson, L., Peng, Shia-Hui: A hybrid LES-RANS model based on a one-equation SGS model and a two-equation  $k-\omega$  model. *Proc. Symp. on Turbulence and Shear Flow Phenomena, Second Int. Symp.*, KTH, Stockholm, vol. 2, pp. 175–180 (2001)
9. Deardorff, J.W.: The use of subgrid transport equations in a three-dimensional model of atmospheric turbulence. *J. Fluid Eng. ASME* **95**, 429–438 (1973)

10. Dejoan, A.: *Simulation de grandes échelles turbulentes en écoulement de canal plan soumis à des perturbations instationnaires*. Dissertation, Université d'Aix-Marseille II (1998)
11. Dejoan, A., Schiestel, R.: Simulation de grandes échelles en écoulement turbulent soumis à des perturbations instationnaires. *Actes du 14<sup>ème</sup> Congrès Français de Mécanique, AUM, Toulouse*. Communication réf. 453, 30 August–3 September (1999)
12. Dejoan, A., Schiestel, R.: Large eddy simulations of non-equilibrium flows using transport equations subgrid scale model. *Proc. Symp. on Turbulence and Shear Flow Phenomena, Second Int. Symp.*, KTH, Stockholm, vol. 2, pp. 341–346 (2001)
13. Dejoan, A., Schiestel, R.: LES of unsteady turbulence via a one-equation subgrid scale transport model. *Int. J. Heat Fluid Flow* **23**, 398–412 (2002)
14. Deschamps, V.: Simulation numérique de la turbulence dans un écoulement de canal plan. *La Recherche Aérospatiale* **3**, 37–52 (1989)
15. Feng, M., Tardu, S., Binder, G.: Inner region of unsteady channel flow. In: So R.M.C., Speziale C.G., Launder B.E. (eds.) *Near wall turbulent flows*. Elsevier New York (1993)
16. Germano, M., Piomelli, U., Moin, P., Cabot, W.H.: A dynamic subgrid-scale eddy viscosity model. *Phys. Fluids A* **3**(7), 1760–1765 (1991)
17. Hamba, F.: An attempt to combine large eddy simulation with the  $k$ -epsilon model in a channel flow calculation. *Theor. Comput. Fluid Dyn.* **14**(5), 323–336 (2001)
18. Hamba, F.: A hybrid RANS/LES simulation of turbulent channel flow. *Theor. and Comput. Fluid Dyn.* **16**(5), 387–403 (2003)
19. Hanjalic, K., Hadziabdic, M., Temmerman, L., Leschziner, M.: Merging LES and RANS strategies: zonal or seamless coupling? In: *Direct and Large-Eddy Simulation n°V (Proceedings of the Fifth International ERCOFTAC Workshop on Direct and Large-Eddy Simulation*. Held at the Munich University of Technology, Germany, August 27–29, Friedrich, R., Geurts, B., Métais, O. (eds.), *Ercoftac series vol. 9*, Kluwer, Dordrecht, pp. 451–464 (2004)
20. Hinze, J.O.: *Turbulence*, 2nd edn. McGraw-Hill, New York (1975)
21. Horiuti, K., Yoshizawa, A.: Large-eddy simulation of turbulent channel flow by 1-equation model. In: Schumann, U., Friedrich R. (eds.) *Notes on Numerical Fluid Mechanics vol. 15. Direct and Large-eddy Simulation of Turbulence. Proc. EUROMECH Coll. No 199*, Munich, 1985. Vieweg-Verlag Wiesbaden, pp. 119–134 (1986)
22. Hughes, T.J.R., Oberai, A.A., Mazzei, L.: Large eddy simulation of turbulent channel flow by the variational multiscale method. *Phys. Fluids* **13**(6), 1784–1799 (2001)
23. Hussain, A.K.M.F., Reynolds, W.C.: Measurements in fully developed turbulent channel flow. *J. Fluids Eng. Trans. ASME* **1** **97**, 568–578 (1975)
24. Jones, W.P., Launder, B.E.: The prediction of laminarization with a two-equation model of turbulence. *Int. J. Heat Mass Transf.* **15**, 301–313 (1972)
25. Krajnovic, S., Davidson, L.: A mixed one-equation subgrid scale model for large eddy simulation. *Int. J. Heat Fluid Flow* **23**, 413–425 (2002)
26. Kwak, D., Reynolds, W.C., Ferziger, J.H.: Three-dimensional time-dependent computation of turbulent flows. Dept. of Mech. Eng., Stanford Univ., Calif., Report TF-5 (1975)
27. Laufer, J.: Investigation of turbulent flow in a two-dimensional channel. NACA Report 1053 (1951)
28. Launder, B.E., Sharma, B.I.: Application of the energy-dissipation model of turbulence to the calculation of flow near a spinning disc. *Lett Heat Mass Transf.* **1**, 131–138 (1974)
29. Lesieur, M.: *Turbulence in fluids*, 2nd edn. . Kluwer Dordrecht (1990)
30. Métais, O., Lesieur, M.: Spectral large-eddy simulation of isotropic and stably stratified turbulence. *J. Fluid Mech.* **125**, 475–503 (1992)
31. Moin, P., Kim, J.: Numerical investigation of turbulent channel flow. *J. Fluid Mech.* **118**, 341–377 (1982)
32. Moser, R.D., Kim, J., Mansour, N.N.: Direct numerical simulation of turbulent channel flow up to  $Re_\tau = 590$ , *Phys. Fluids* **11**(4), 943–945 (1999)
33. Nikitin, N.V., Nicoud, F., Wasistho, B., Squires, K.D., Spalart, P.R.: An approach to wall modeling in large-eddy simulations. *Phys. Fluids Letters* **12**(7), 1629–1632 (2000)
34. Patel, V.C., Rodi, W., Scheuerer, G.: Turbulence models for near wall and low Reynolds number flows: a review. *AIAA J* **23**(9), 1308–1319 (1985)
35. Piomelli, U., Balaras, E., Pasinato, H., Squires, K.D., Spalart, Ph.R.: The inner-outer interface in large eddy simulations with wall-layer models. *Int. J. Heat Fluid Flow* **24**, 538–550 (2003)
36. Piomelli, U., Moin, P., Ferziger, J.H.: Model consistency in large eddy simulation of turbulent channel flow. *Phys. Fluids* **31**(7), 1884–1891 (1988)
37. Rubinstein, R., Zhou, Ye: Analytical theory of the destruction terms in dissipation rate transport equations. *Phys. Fluids* **8**(11), 3172–3178 (1996)
38. Rubinstein, R., Zhou, Ye: Schiestel's Derivation of the epsilon equation and two equations modeling of rotating turbulence. NASA/CR-2001-211060, *ICASE Report No 2001-24*, pp. 1–6 (2001)
39. Sarkar, A., So, R.M.C.: A critical evaluation of near-wall two-equation models against direct numerical simulation data. *Int. J. Heat Fluid Flow* **18**(2), 197–208 (1997)
40. Schiestel, R.: Sur la modélisation des écoulements turbulents en non-équilibre spectral. *C.R. Acad. Sci., Paris*, **302**, series II, (11), pp. 727–730 (1986)
41. Schiestel, R.: Multiple time scale modeling of turbulent flows in one point closures. *Phys. Fluids* **30**(3), 722–731 (1987)
42. Schiestel, R.: *Les écoulements turbulents, modélisation et simulation*, 2nd edn. Hermès Paris (1998)

43. Schiestel, R., Viazzo, S.: A Hermitian-Fourier numerical method for solving the incompressible Navier–Stokes equations. *Comput Fluids* **24**(6), 739–752 (1995)
44. Schumann, U.: Subgrid scale model for finite difference simulations of turbulent flows in plane channels and annuli. *J. Comp. Phys.* **18**, 367–404 (1975)
45. Scotti, A., Meneveau, C., Lilly, D.K.: Generalized Smagorinsky model for anisotropic grids. *Phys. Fluids A* **5**(9), 2306–2308 (1975)
46. Scotti, A., Piomelli, U.: Numerical simulation of pulsating turbulent channel flow. *Phys. Fluids* **13**(5), 1367–1384 (2001)
47. Scotti, A., Piomelli, U.: Turbulence models in pulsating flows. *AIAA J* **40**(3), 537–544 (2002)
48. Spalart, P.R., Jou, W.H., Strelets, M., Allmaras, S.R.: Comments of the feasibility of LES for wings, and of a hybrid RANS/LES approach. First AFOSR Int. Conf. On DNS/LES, Ruston, LA, 4–8, August 1997. In: Liu, C., Liu Z. (eds.) *Advances in DNS/LES*. Greyden Columbus, OH (1997)
49. Tardu, S.: Control of drag reduction by time-space periodical suction and blowing. *Proc. 11th Symp. on Turbulent Shear Flows*, Grenoble, September 1997, pp. 9.1–9.6 (1997)
50. Tardu, S., Binder, G.: Wall shear stress modulation in an unsteady turbulent channel flow with height imposed frequencies. *Phys. Fluids A* **5**(8), 2028–2037 (1993)
51. Tardu, S., Binder, G., Blackwelder, R.: Turbulent channel flow with large amplitude velocity oscillations. *J. Fluid Mech.* **267**, 109–151 (1994)
52. Travin, A., Shur, M., Strelets, M., Spalart, P.R.: Physical and numerical upgrades in the detached eddy simulations of complex turbulent flows. In: Friedrich, R., Rodi W. (eds.) *Advances in LES of Complex Flows*. Kluwer Dordrecht, pp. 239–254 (2002)
53. Vasilyev, O.V., Lund, T.S., Moin, P.: A General class of commutative filters for LES in Complex Geometries. *J. Comput. Phys.* **146**, 82–104 (1998)
54. Viazzo, S., Schiestel, R.: Simulations des grandes échelles turbulentes en canal à l’aide d’un schéma hermitien. *Comptes Rendus de l’Académie des Sciences*, **321**, series IIB, pp. 225–232 (1995)
55. Wei, T., Willmarth, W.: Examination of V-Velocity Fluctuations in a Turbulent Channel Flow in the Context of Sediment Transport. *J. Fluid Mech.* **223**, 241–252 (1991)

Copyright of Theoretical & Computational Fluid Dynamics is the property of Springer - Verlag New York, Inc. and its content may not be copied or emailed to multiple sites or posted to a listserv without the copyright holder's express written permission. However, users may print, download, or email articles for individual use.